HHS Public Access

Author manuscript

Cell Rep. Author manuscript; available in PMC 2022 April 21.

Published in final edited form as:

Cell Rep. 2022 March 01; 38(9): 110448. doi:10.1016/j.celrep.2022.110448.

CDK/cyclin dependencies define extreme cancer cell-cycle heterogeneity and collateral vulnerabilities

Erik S. Knudsen[1,7,*], **Vishnu Kumarasamy**[1,2], **Ram Nambiar**[1,2], **Joel D. Pearson**[3], **Paris Vail**[1,2], **Hanna Rosenheck**[1,2], **Jianxin Wang**[2], **Kevin Eng**[2], **Rod Bremner**[3], **Daniel Schramek**[3], **Seth M. Rubin**[4], **Alana L. Welm**[5], **Agnieszka K. Witkiewicz**[2,6,*]

[1]Department of Molecular and Cellular Biology, Roswell Park Cancer Center, Buffalo, NY 14203, USA

[2]Department of Cancer Genetics and Genomics, Roswell Park Cancer Center, Buffalo, NY 14203, USA

[3]Lunenfeld Tanenbaum Research Institute, Toronto, ON M5G 1X5, Canada

[4]Department of Chemistry and Biochemistry, University of California, Santa Cruz, Santa Cruz, CA 95064, USA

[5]Department of Oncological Sciences, Huntsman Cancer Institute, University of Utah, Salt Lake City, UT 84112, USA

[6]Department of Pathology, Roswell Park Cancer Center, Buffalo, NY 14203, USA

[7]Lead contact

SUMMARY

Progression through G1/S phase of the cell cycle is coordinated by cyclin-dependent kinase (CDK) activities. Here, we find that the requirement for different CDK activities and cyclins in driving cancer cell cycles is highly heterogeneous. The differential gene requirements associate with tumor origin and genetic alterations. We define multiple mechanisms for G1/S progression in RB-proficient models, which are CDK4/6 independent and elicit resistance to FDA-approved inhibitors. Conversely, RB-deficient models are intrinsically CDK4/6 independent, but exhibit differential requirements for cyclin E. These dependencies for CDK and cyclins associate with gene expression programs that denote intrinsically different cell-cycle states. Mining therapeutic

*Correspondence: agnieszka.witkiewicz@roswellpark.org (A.K.W.), erik.knudsen@roswellpark.org (E.S.K.).

AUTHOR CONTRIBUTIONS

Conceptualization, E.S.K., V.K., S.M.R., and A.K.W. Methodology, E.S.K., V.K., R.N., J.D.P., H.R., J.W., K.E., R.B., D.S., S.M.R., A.L.W., and A.K.W. Formal analysis, R.N., V.K., P.V., J.W., and K.E. Investigation, V.K., R.N., P.V., H.R., and J.W. Resources/ funding, E.S.K., J.D.P., H.R., R.B., S.M.R., A.L.W., and A.K.W. Writing – original draft, review, & editing, E.S.K., V.K., R.N., J.D.P., H.R., J.W., K.E., R.B., D.S., S.M.R., A.L.W., and A.K.W. Visualization, E.S.K., V.K., R.N., P.V., H.R., J.W., and A.K.W. Supervision, E.S.K., R.B., D.S., S.M.R., A.L.W., and A.K.W.

SUPPLEMENTAL INFORMATION

Supplemental information can be found online at https://doi.org/10.1016/j.celrep.2022.110448.

DECLARATION OF INTERESTS

A.L.W. has received royalties from licenses of patient-derived xenograft or organoid models issued by the University of Utah. The university may issue new licenses in the future at its discretion, which may result in additional royalties. E.S.K. and A.K.W. have served on the BioVica scientific advisory board.

sensitivities shows that there are reciprocal vulnerabilities associated with RB1 or CCND1 expression versus CCNE1 or CDKN2A. Together, these findings illustrate the complex nature of cancer cell cycles and the relevance for precision therapeutic intervention.

Graphical abstract

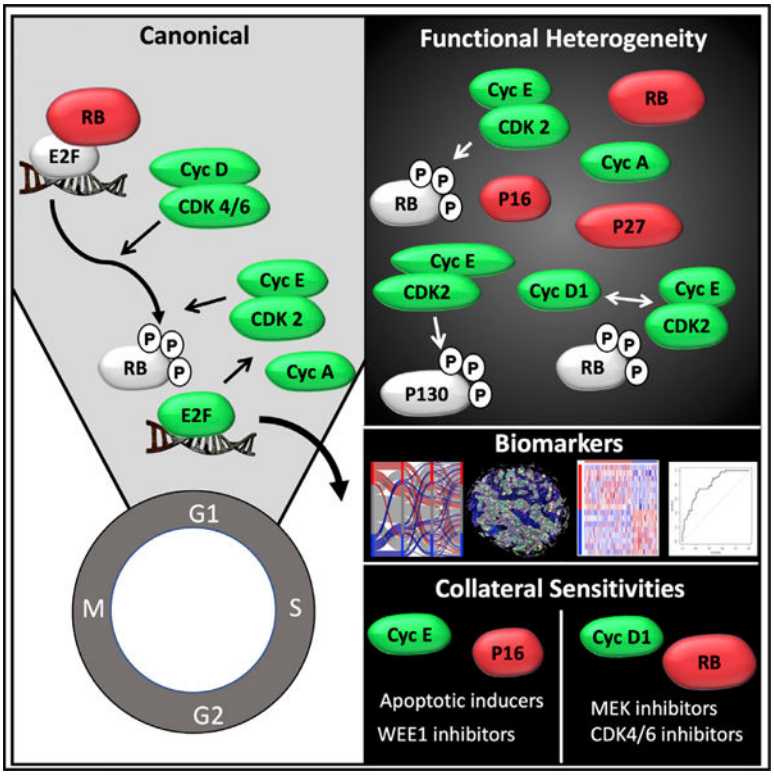

In brief

Knudsen et al. find that there is extensive heterogeneity in the requirement for CDK and cyclins across cancer models. Multiple biochemically distinct mechanisms drive cell division. Divergent cell-cycle states harbor distinct genetic and pharmacological vulnerabilities, suggesting that cell-cycle diversity could be exploited for a precision approach to cancer therapy.

INTRODUCTION

The cell cycle is driven by the action of cyclin-dependent kinases (CDKs) (Hartwell and Kastan, 1994; Malumbres and Barbacid, 2001; Nurse, 2012; Sherr, 1996). Conventionally, D-type cyclins (cyclins D1, D2, or D3) accumulate in response to physiological mitogenic signals or oncogenic signals that drive cellular proliferation (Diehl, 2002; Sherr, 1995). These cyclins preferentially interact with CDK4 or CDK6 to produce active complexes. The CDK4/6 catalytic activity is considered key for initiating progression through G1/S phases of the cell cycle, which is mediated by these kinases driving the phosphorylation of the retinoblastoma (RB) tumor suppressor and related proteins (p107 and p130) (Burkhart and Sage, 2008; Knudsen et al., 2019; Weinberg, 1995). The RB family of proteins function as

transcriptional corepressors and serve to inhibit proliferation by impeding the expression of genes required for cell-cycle progression that are under the control of the E2F family of transcription factors or FOXM1 (Nevins, 2001; Sadasivam and DeCaprio, 2013). Tumors that lack the RB tumor suppressor are CDK4/6 independent (Dean et al., 2010; Finn et al., 2009; Knudsen and Witkiewicz, 2016) and resistant to pharmacological CDK4/6 inhibitors such as palbociclib (Bertucci et al., 2019; Finn et al., 2009; O'Leary et al., 2018a). Consistent with this resistance, many RB-deficient tumors express high levels of the CDK4/6 inhibitor $p16^{ink4a}$ (Witkiewicz et al., 2011; Xiong et al., 1993). These data support the concept that RB represents the key substrate for CDK4/6 complexes in driving cell division.

In addition to CDK4/6, CDK2 plays an important role in coordinating cell-cycle progression (Coverley et al., 2002; Sherr, 2000). CDK2 through binding with cyclin E or cyclin A can promote cell-cycle progression in G1, S, or G2 phases of the cell cycle. While CDK2 can ostensibly phosphorylate RB (Hinds et al., 1992), CDK4/6 is viewed as priming the phosphorylation of RB (Narasimha et al., 2014). The exact relationship of CDK4/6 and CDK2 in driving the hyperphosphorylation of RB remains unclear, and mono- and partially phosphorylated forms of RB further complicate what has been largely viewed as a binary switch for proliferation (Narasimha et al., 2014; Rubin et al., 2020; Sanidas et al., 2019). Against these findings, the specific requirement and/or sufficiency of CDK2 in driving the phosphorylation of RB and cell-cycle progression has remained unclear, with differential results that could be a reflection of cellular context (Tetsu and McCormick, 2003). RB activation can act to limit the activity of CDK2 by controlling the expression of cyclin E and cyclin A (DeGregori et al., 1995; Johnson and Schneider-Broussard, 1998; Knudsen et al., 1999; Leng et al., 1997). Thus, conventionally, the cell cycle is considered relatively linear, wherein CDK4/6, through the phosphorylation of RB and related proteins, controls the activity of CDK2 as summarized in multiple reviews (Goel et al., 2018; Knudsen et al., 2019; Sherr, 1996; VanArsdale et al., 2015).

While there is substantial biochemical data that supports the linear model of cell-cycle progression, studies in mice and other systems have questioned the rigidity of these relationships (Barriere et al., 2007; Kozar et al., 2004; Malumbres and Barbacid, 2006; Malumbres et al., 2004). Mice or human cells can divide in the absence of CDK4/6 or CDK2 in certain instances (Malumbres et al., 2004; Tetsu and McCormick, 2003). These cell-cycle adaptations have also emerged as potential features of resistance to CDK4/6 inhibitors that are used clinically (Herrera-Abreu et al., 2016; Kumarasamy et al., 2020). Notably, RB loss or cyclin E gain are associated with resistance to CDK4/6 inhibitors; different oncogenic permutations also seem to impinge on the cell cycle to limit sensitivity to the pharmaceutical agents (Li et al., 2018; O'Leary et al., 2018b; Turner et al., 2019; Wander et al., 2020). In spite of this plasticity, the majority of tumors are expected to use CDK4/6 and CDK2 to traverse the G1/S transition. Here, we sought to define the spectrum of CDK and cyclin dependencies broadly in cancer cell lines and patient-derived models with complementary biochemical analyses. Together, these findings indicate multiple different cell-cycle states with specific genetic and pharmaceutical vulnerabilities and a high degree of heterogeneity within tumor types.

RESULTS

Diversity of CDK/cyclin dependence in cancer cell lines

Targeting the cell cycle as a means to treat cancer is appealing since deregulated proliferation is achieved mechanistically through mitotic cell division (Asghar et al., 2015; Shapiro, 2006; Suski et al., 2021). The key drivers of the cell cycle are cyclins and CDKs. Conventionally, CDK4 or CDK6 in complex with D-type cycles initiate the phosphorylation of RB in G1 phase of the cell cycle, which is followed by the activation of downstream CDK/cyclin complexes that promote progression through the remainder of the cell cycle (Figure 1A). We used DepMAP data (McFarland et al., 2018; Tsherniak et al., 2017), in which individual genes were targeted by CRISPR-Cas9-mediated deletion to assess the functional requirements of CDK and cyclin genes across 717 cell lines. The CERES score is a corrected measure of essentiality, in which scores of −1 to −2 are generally associated with genes that are considered essential for proliferation. There was a subset of CDKs and cyclins that are involved in transcription (e.g., CDK7, CDK9) and other processes that have distinct vulnerabilities (Figure S1). However, cell-cycle regulators coalesce into two general behaviors (Figures 1B and S1). The genes CCNA2 and CDK1 are essentially universally required, which is consistent with general expectations, but distinct from the compensation that has been observed in select models (Diril et al., 2012; Gopinathan et al., 2014; Kalaszczynska et al., 2009) (Figure 1B). In contrast, for other cell-cycle genes, there was a diversity of responses to their deletion, in particular, genes that regulate the G1/S transition (CDK4, CDK6, CCND1, CDK2, and CCNE1) yield particularly variant vulnerabilities (Figures 1B and S1). There were also a number of CDK genes that are not associated with significant vulnerability; for example, CDK3 and CDK5 (Figure S1). We focused the further analyses on the CDK and cyclins that promote G1/S progression, maintaining CDK1 and CCNA2 as controls for the efficacy of gene targeting. The diversities of sensitivity were borne out in different tumor cell types (Figures 1C and S2). Clustering cell lines based on vulnerabilities defined 6 distinct groups of cells that could be broadly categorized by sensitivity to loss of a particular CDK or Cyclin, with the invariant dependence on CDK1 and CCNA2 (Figure 1D). These data were associated with certain genetic configurations of the cell lines (Figure 1D); for example, most of the RB1-deficient tumor lines are in clusters 3 and 4, with CDKN2A loss excluded. Similarly, most of the CCNE1 amplifications occurred in cluster 3 (Figure 1E). To investigate potential genetic drivers, the enrichment of specific oncogenic events was compared across the clusters (Figure S3). These data illustrate that across the clusters, there were few oncogenic events that were selective, with the exception of enrichment for TP53 mutations in cluster 4, fewer epidermal growth factor receptor (EGFR) mutations in cluster 1, and few MYC amplifications in cluster 5.

Tumor-type selective dependence on CDKs/cyclins

Statistical analyses of the clusters revealed that they harbored distinct dependencies on select CDK or cyclin genes. Four clusters were dependent on CDK4, CDK6, or CCND1 (clusters 1, 2, 5, and 6) (Figure 2A). One cluster was more dependent on CCNE1 (cluster 3), and one cluster was minimally dependent on these G1/S CDKs and cyclins (cluster 4). Importantly, the dependence on CDK1 and CCNA2 was observed across all clusters, indicating that the disparity in sensitivity is not due to a technical limitation of

gene targeting (Figure 2A). Statistical analyses and clustering confirmed the relationships between CDK4, CDK6, CCND1, and CCNE1 (Figure 2B). Interrogating the relationship of these clusters with specific disease types illustrated that there were significant enrichments that are likely relevant for targeting specific cancers with select classes of CDK inhibitors. For example, breast cancer cell lines were enriched within cluster 2 (Figure 2C). In contrast, ovarian and endometrial cancers were enriched in cluster 3 (Figure 2C). Cluster 4 harbored all of the cervical cancer cell lines, suggesting that such human papillomavirus (HPV)-driven tumors may be largely refractory to the inhibition of a single G1/S CDK (Figure 2C). It should be noted that while there is enrichment for dependency, in most tumor types there is heterogeneity, in which there are cell lines that fall into multiple clusters. These enrichments mapped to individual gene dependencies (Figures 2D–2F and S4). For example, neuroblastoma and melanoma are highly dependent on CCND1, breast cancer, and melanoma on CDK4 and leukemia and myeloma on CDK6 (Figure 2D). A number of other differential and enrichments were observed; for example, a dependence of brain cancer on CCND3 and CDK2 and (Figure S4). The main differentiating factor between clusters 1 and 5 was the relative requirement for CCND1. This is likely due to vulnerability in cluster 5 for CCND2 and CCND3 depletion in hematological malignancies (Figure 2E). Lastly, gynecological malignancies were enriched for dependency on CCNE1 and CDK2, which is consistent with the high level of CCNE1 amplification that is found in such tumor types (Figure 2F).

Differential CDK/cyclin complexes delineate vulnerability profiles

To interrogate the relevance of these clusters with sensitivity to CDK4/6 inhibitors that are applied clinically, we used the published half-maximal inhibitory concentration (IC_{50}) data of palbociclib and abemaciclib for breast cancer (O'Brien et al., 2018) and ovarian cancer cell lines (Konecny et al., 2011). In both classes of cell lines, there was an enrichment for cluster 2 (dependent on CDK4 and CCND1) for sensitivity, while clusters 3 and 4 were associated with resistance (Figure 3A). Clusters 5 and 6 exhibited intermediate IC_{50}s (Figure 3A). To mechanistically explore the gene dependencies and the relationship to pharmaceutical intervention, we used a panel of breast cancer cell lines that encompasses multiple clusters and harbors distinct genetic features (Figure 3B). Initially, we used palbociclib with live cell imaging that confirmed the data with published IC_{50} data. MCF7 are sensitive to palbociclib, while HCC1806, MB157, MB436, and MB468 are resistant (Figure S5). To determine how RB-proficient tumor models escape CDK4/6 inhibition, we used MB157 and HCC1806 cell lines. MB157 is in cluster 3, which harbors a vulnerability to the loss of CCNE1. Depleting CCNE1 using RNAi resulted in the robust inhibition of cell proliferation (Figure 3C). Biochemically, the loss of cyclin E was associated with the dephosphorylation of RB and subsequent reduction in cyclin A expression as a downstream target gene (Figure 3C). CCNE1 amplification in MB157 uncouples CDK4/6 from cell-cycle progression as indicated by persistent RB phosphorylation and cyclin A expression following the depletion of these kinases (Figure S5). Consistent with the biochemical data, the cells continued proliferating following the knockdowns of CDK4 and CDK6, as indicated by live cell imaging and bromodeoxyuridine (BrdU) incorporation (Figures 3D and S5). The other RB-proficient breast cancer cell line, HCC1806, also harbors CCNE1 amplification and is resistant to palbociclib (Figure S5). However, our analysis indicates that

they fall under a different cluster (cluster 6), in which the cell cycle is dependent on cyclin D1. Consistent with this, CCND1 knockdown in HCC1806 cells blocked cell proliferation, without modulating the effect of palbociclib (Figure 3E). To delineate the functional role of cyclin D1 on the cell-cycle machinery of HCC1806 cells, we interrogated its interaction with multiple CDKs by co-immunoprecipitation. In the actively proliferating HCC1806 cell line, cyclin D1 does not form an apparent complex with CDKs, including CDK4, CDK6, CDK2, and CDK1, while only an interaction with $p27^{KIP1}$ was observed (Figures 3F and S5). MCF7 cells were included as a comparator that harbors conventional cyclin D1/CDK4 and cyclin D1/$p27^{KIP1}$ complexes (likely as a trimer) (Figure 3F). The lack of apparent cyclin D1/CDK complexes in HCC1806 cells was further interrogated by *in vitro* kinase reactions, in which no cyclin D1-associated kinase activity was detected based on the phosphorylation status of an exogenous RB substrate (Figure 3G). Additional data illustrated that the proliferation of HCC1806 cells does not require an active CDK4, which makes them discrete from MCF7 cells, in which the presence of this kinase is critical (Figure S5). These analyses suggest a non-canonical function of cyclin D1 to drive the proliferation of HCC1806 cells in the absence of a clearly definable catalytic complex. Knockdown of cyclin D1 in HCC1806 cells resulted in the accumulation of $p27^{KIP1}$ protein, which interacts with CDK2 and cyclin E1 and limits the CDK2 kinase activity, which could contribute to the growth arrest (Figures 3H and 3I). Depletion of $p27^{KIP1}$ is sufficient to partially rescue the cell-cycle arrest induced by cyclin D1 knockdown, supporting the supposition that the principal requirement of cyclin D1 in this cell line is to titrate $p27^{KIP1}$ (Figure S5). These data define several distinct RB-positive cell cycles as summarized in Figure 3J.

Although HCC1806 cells harbors high cyclin E1 levels, they are not vulnerable to the loss of CCNE1, which makes this model distinct from MB157. Co-immunoprecipitation revealed that the depletion of cyclin E1 results in the formation of cyclin D1/CDK4 complex, which could impart resistance to CCNE1 depletion (Figure S5). Consistent with this observation, concurrent knockdowns of CDK4 and cyclin E1 resulted in a growth arrest, indicating the compensatory role of CDK4 (Figure S5). Moreover, CCNE1 depletion in HCC1806 cells renders this model to be sensitive to palbociclib (Figure S4). Thus, there are specific tumor models in which CCNE1 amplification yields distinct phenotypic effects.

It is widely believed that RB loss represents a singular form of cell-cycle deregulation. As expected, the RB-deficient models MB436 and MB468 were resistant to the depletion of CCND1, CDK4, and CDK6 (Figures 4A and S6). In addition, as with HCC1806, cyclin D1 did not bind to CDK4, but in the RB-deficient models, cyclin D1 also did not bind to $p27^{KIP1}$. Presumably, this was due to the high expression of $p16^{INK4A}$ in these RB-deficient models (Figure 4B). These data suggest that other CDK-cyclins are driving the cell cycle of RB-deficient models. The RB-deficient cell models are present in clusters 3 or 4, which are differentiated based on the sensitivity to CCNE1 depletion. The MB436 model is cyclin E dependent, while MB468 is cyclin E independent (Figure 4C). A feature of cluster 4 is the presence of cervical cancer cell lines that harbor HPV-E7, which is known to inactivate the RB and the related proteins p107 and p130 (Goodwin and DiMaio, 2000; Ludlow and Skuse, 1995). Therefore, we interrogated potential differences in cell-cycle circuits involving p130. These data revealed that in MB436, p130 phosphorylation is cyclin E dependent, while in MB468 cells, p130 phosphorylation is independent of cyclin E (Figure 4D). The functional

role for p130 was determined by knockdown and subsequent impact on downstream targets cyclin A, cyclin B1, and CDK1 (Figure 4E). Consistent with these findings, CDK2 activity as determined with a sensor and conventional *in vitro* kinase assay, is CCNE1 dependent in MB436 cells but CCNE1 independent in MB468 (Figures 4F and S6). Together, these data suggest that in specific settings, the loss of RB obviates a requirement for both CDK4/6 and cyclin E in driving the cell cycle. Interestingly, this epistatic relationship could also be observed in MB157 cells, where the specific deletion of RB1 altered the subsequent requirement for CCNE1 and CDK2 in cell division (Figures 4G and 4H). In this setting, p130 is still largely dephosphorylated, but apparently not sufficient in the absence of RB to fully suppress proliferation (Figure 4I). While resistant to CCNE1 depletion, MB468 cells are sensitive to CCNA2 depletion or treatment with PF-06873600 (a CDK4/6/2/1 inhibitor) (Figure S6). Thus, MB468 are CDK dependent, albeit with little apparent requirement for conventional G1/S regulatory mechanisms.

Gene expression features associated with CDK/cyclin vulnerability

To identify putative gene expression associated with sensitivity to CDK or cyclin depletion, we used RNA sequencing data for the cell lines (Figures 5, S7, and S8). Due to the clinical relevance of CDK4/6 inhibitors, we focused on the comparison of CDK4- or −6-sensitive solid tumor models (clusters 1 and 2) versus those that were resistant (clusters 3 and 4). There were a large number of differentially expressed genes between the clusters. Gene set enrichment analysis (GSEA) illustrated that the clusters were highly associated with ‘‘hallmark’’ features, including RAS pathway and the epithelial-to-mesenchymal transition (Figures 5A and S7). In addition to these features, a particularly dominant gene expression feature shown in the volcano plot was the expression of the CDK or cyclin that is associated with the vulnerability (Figures 5B–5E and S8). For example, the predominant gene expression differences between cluster 1 and 2 compared with 3 were CCNE1 and CCND1 (Figures 5B and 5D). In addition, CDKN2A (the endogenous CDK4/6 inhibitor) and RB1 emerged as the top genes associated with the differences between clusters 1 and 2 compared with 3 and 4 (Figures 5B–5E). These data support the concept that while there are substantial biological differences that could be driving dependencies, the intersection of cyclin gene expression with RB1 and CDKN2A is relevant to the resultant vulnerabilities.

To define the predictive gene expression markers for a given genetic vulnerability, we used logistic regression analyses of the top 10 differentially expressed genes between clusters (Figures 5F–5G and S9). A stepwise algorithm was used to filter irrelevant genes that do not contribute to prediction. This approach gave rise to specific weighted classifiers associated with dependency for cyclin D1 or cyclin E. These classifiers were used with the breast cancer and ovarian cancer IC_{50} data to predict sensitivity and resistance, respectively, to palbociclib (Figures 5E, 5F, S9, and S10).

Discordant cell-cycle states

Together, the data above suggest that there are distinct cell-cycle states that can be largely predicted by gene expression differences. Conventionally, cyclin D1 would be expected to contribute to cyclin E expression by initiating the phosphorylation of RB and derepression of E2F (Goel et al., 2018; Knudsen et al., 2019; Sherr, 1996; VanArsdale et al., 2015). This

trend was observed in colon and pancreatic cancer cell lines (Figures 6A and S11) However, in many tumor types, cyclin D1 and cyclin E expressions were inversely correlated (Figures 6B and S11). This finding was similar to the inverse relationship of CDKN2A and RB1 expression cell lines (Figures 6B and S11). These findings suggest the possibility of two relatively large and distinct tumor populations—those driven by cyclin D1 with RB intact and those driven by cyclin E and/or with RB compromised. These inverse relationships are apparent in The Cancer Genome Atlas (TCGA) data as well as the cell lines (Figures 6C and S11). Analysis of gene expression quantiles using clusters not confounded by CCND2 or CCND3 (clusters 1, 2, 3, 4, and 6) illustrated that very few cells were consistently high or low for each gene, as summarized in the Sankey plot (Figure 6D).

As a complementary strategy, we optimized multispectral immunofluorescence for staining triple negative breast cancer (TNBC) tumor tissues (Adams et al., 2018). This panel includes antibodies against cyclin D1, cyclin E, and phospho-RB (Ser 807/811) (Figures 6E and S12). In the analyses of 149 TNBC cases, we found a distribution of discrete cell-cycle states as shown by the clustering of the protein levels (Figure S12). Dual positive cyclin D1 and cyclin E high tumors were relatively rare, compared to tumors dominated by a single cyclin. Together, these data reinforce the concept of fundamentally different cell-cycle states that in principle could harbor distinct collateral vulnerabilities.

Collateral therapeutic vulnerabilities associated with cell-cycle states

In investigating genetic vulnerabilities that were associated with high or low gene expression, we found that CCNE1, CCND1, RB1, and CDKN2A revealed reciprocal relationships (Figures 6F, S13, and S14). For example, genes whose deletion represented a specific vulnerability in cyclin D1 high tumor cells were generally associated with resistance in cyclin E high tumor cells. This relationship is summarized in the Sankey blots for both CCND1/CCNE1 and RB1/CDKN2A (Figures 6G and S15). Mining the pathways associated with vulnerabilities revealed both expected and unexpected dependencies. For example, CCNE1 high cell lines harbored vulnerability to CDK2, SKP2, and CKS1B, as may be expected as effectors of CCNE1 function (Figure 6H). Given the noted role of CCNE1 in driving replication stress (Bartkova et al., 2006; Jones et al., 2013), there were selective sensitivities to multiple genes involved in DNA replication (e.g., CDT1, CDC45). However, the CCNE1 high cell lines were unexpectedly selectively sensitive to multiple polycomb repressor complex (PRC) subunits EED, EZH2, E2F3, and EP300, as illustrated in network analysis. Similar reciprocal vulnerabilities were observed between RB and CDKN2A high expressing cell lines (Figure S15).

To understand the broader therapeutic implications of these findings, drug sensitivity data from the Cancer Cell Line Encyclopedia associated with the cell lines was stratified by gene expression for CCND1, CCNE1, RB1, and CDKN2A. This approach yielded a relatively small set of consistent drug vulnerabilities as summarized in the heatmaps (Figure 7A). As expected, CDK4/6 inhibitor sensitivity was associated with the high expression of CCND1 and RB1, while resistance was associated with the high expression of CDKN2A and CCNE1 (Figures 7B and 7C). CCNE1 and CDKN2A high tumor cell lines were largely resistant to MEK inhibitors present in the dataset (Figures 7B and 7C). In contrast, such tumor cells

were selectively sensitive to the WEE1 inhibitor MK1775 and the survivin inhibitor YM155 (Figures 7B and 7C). When we evaluated these data, it appeared that there were distinctions between CDKN2A high and CCNE1 high tumors. Notably, CDKN2A high/RB low tumor cells exhibit sensitivity to microtubule poisons, Polo-like kinase 1 (PLK1) inhibitors, aurora kinase (AURK) inhibitors, and B cell leukemia/lymphoma 2 (BCL2) inhibitors, relative to CCNE1 high tumors (Figures S16 and S17). Conversely CDKN2A high tumors are particularly resistant to MDM2/4 inhibitors compared with CCNE1, RB, or CCND1 high cell lines (Figure S16). This is likely due to the high mutation of p53 in the CDKN2A high/RB low cell lines (Figure S17). Independent analysis based on RB mutations using the data from the Genomics of Drug Sensitivity further validated the vulnerabilities associated with RB loss (Figure S17).

To explore *in vivo* responses, we investigated how the expression of cell-cycle genes correlated with response to treatment in the patient-derived xenograft (PDX) cohorts from Gao et al. (2015) (Figures 7D and S18). This cohort was largely treated with cytostatic agents. The upper quartiles of CCND1, RB1 compared with CCNE1, and CDKN2A largely recapitulated the behaviors observed in cell culture (Figures 7D and S15). These relationships were also observed with CDK4/6 combinations with MEK and mammalian target of rapamycin (mTOR) inhibitors (Figure 7D), suggesting that cell-cycle gene expression programs harbor dominant relationships over not only single agents but also combination therapies. To further interrogate these findings, we used a panel of TNBC PDX models (Figures 7E and 7F) (DeRose et al., 2011). The RB-proficient model HCI-009 is responsive to the combination CDK4/6 + mTOR inhibition (Figure 7F). In contrast, all of the RB-deficient models (HCI-010, HCI-012, and HCI-015) were resistant to this combination (Figure 7F). In total, these *in vivo* studies reinforce the role of RB in coordinating cytostatic responses to single-agent and select combination therapies. To interrogate sensitivities in tumor models that would be resistant to MEK and CDK4/6 inhibitors, we used isogenic models, in which RB was deleted in breast cancer cell lines. In the MCF7 cell line, the RB-deleted cells were more sensitive to YM155 and alisertib and the combination (Figure 7G). In the MB231 model, RB-deletion facilitated sensitivity to alisertib (Figure 7G). However, the RB-deleted cells were not more sensitive to YM155 and MK177, but such agents were cooperative with alisertib in the RB-deleted models (Figure 7G). Similar findings were observed using other combinations that target survival (navitoclax) and cell-cycle regulatory processes (Figure S18). Together, these data suggest that targeted combination approaches can be used against specific cell-cycle states that are resistant to agents that have a cytostatic mechanism of action.

DISCUSSION

The cell cycle is a well-studied process, with significant data supporting both canonical CDK4/6-RB-CDK2 coupling (Goel et al., 2018; Knudsen et al., 2019; Sherr, 1996; VanArsdale et al., 2015) and adaptations through which this pathway can be distorted (Alvarez-Fernandez and Malumbres, 2020; Herrera-Abreu et al., 2016; Knudsen and Witkiewicz, 2017; Kumarasamy et al., 2020). Here, using a broad panel of cell lines, we believe that it is apparent that there are multiple intrinsic cell-cycle states in cancer cells. While specific observations can be trivialized, such as the universal dependence on CDK1/

CCNA2 or lack of impact of CDK3/CDK5, it should be noted that the literature is full of contradictory conclusions related to the functional significance of veritably all CDK/cyclins (Diril et al., 2012; Gopinathan et al., 2014; Kalaszczynska et al., 2009; Pozo et al., 2013; Tetsu and McCormick, 2003). Using clustering algorithms, cancer cells can be differentiated into at least 6 groups. Of these ~50% are dependent on CDK4 or CDK6 for proliferation. The dependence on CDK6 is differentiated through dependence on either cyclin D1 or cyclins D2 or D3. These dependencies are linked to the tissue of origin as well as genetic features of the cancer that arises. Ostensibly, the ‘‘tissue of origin dependencies’’ is at least partially reflective of normal tissue. For example, CDK6 and CCND2 and CCND3 play a larger role in hematopoiesis (Lam et al., 2000; Scheicher et al., 2015; Sicinska et al., 2003), and, correspondingly, leukemia, multiple myeloma, and lymphoma cell lines are more dependent on CDK6, CCND2, and CCND3 than on CDK4 or CCND1. Genetic features appear to be broadly dominant, as resistance to CDK4 or CDK6 can emerge in tumor cells of essentially any lineage with RB loss. Similarly, cyclin E amplification is associated with dependence on the CCNE1 gene, as is observed most frequently in gynecological malignancies.

In spite of these generalizations, the heterogeneity of the cell cycle emerges as being particularly complex. There appear to be multiple functionally independent cell-cycle states that are operable across and within histological tumor types. In the context of breast cancer, there are clearly cell types (e.g., MCF7) that largely conform to a conventional cell cycle with strict dependence on CDK4/6. This can be bypassed by at least 3 mechanisms. First, cyclin E can bypass the requirement for CDK4/6, as shown in the MB157 model, wherein cyclin E drives RB phosphorylation. Second, it appears that in certain settings, as exemplified by the HCC1806 model, there is a complex dependence on cyclin D1 and CDK4/6 that does not conform to a simple standard paradigm. The HCC1806 model is highly dependent on cyclin D1, but resistant to CDK4/6 inhibitors. In this context, it appears that the depletion of cyclin D1 unleashes $p27^{KIP1}$ and the suppression of CDK2 activity. The mechanism related to these complexes and switching of dependencies with knockdown will require further study and analysis of more cell models. For example, how cyclin E depletion results in the assembly of CDK4 complexes’ sensitivity to palbociclib in this model remains unclear. Furthermore, it is likely that other cell lines in this cluster are using different mechanisms to bypass the requirement for CDK4 or CDK6. This heterogeneity is reflected in the differential sensitivity of cells within this cluster to the CDK4/6 inhibitor palbociclib. Third, tumor cells that have lost RB are uniformly resistant to the depletion of CDK4 and CDK6, as well as cyclin D1. While the resistance to CDK4/6 inhibition is well documented, even RB-deficient tumor models have differing CDK and cyclin requirements. One subgrouping is clearly dependent on cyclin E. In this setting cyclin E is driving the phosphorylation of p130 to enable cell-cycle progression. However, there is another group that is largely resistant to the depletion of essentially all of the G1/S regulatory CDKs and cyclins. These models are still sensitive to CDK1 and CCNA2 depletion, suggesting a possible utilization of CDK1 to drive both G1/S and G2/M, as has been observed in mouse models (Santamaria et al., 2007). Interestingly, in cells that are cyclin E addicted, the deletion of RB is sufficient to enable proliferation with cyclin E knockdown. Thus, multiple complex dependencies are intrinsically operable across different tumor types.

A challenge in the clinical use of CDK4/6 inhibitors has been the identification of predictive biomarkers. With unbiased approaches, it emerged that the most potent gene expression features associated with dependence on a CDK or a cyclin was essentially the expression levels of the target and other known members of the network in a reciprocal relationship. For example, cells that are dependent on cyclin D1 generally express high levels of cyclin D1 and RB1, but low levels of cyclin E and CDKN2A. These reciprocal relationships are apparent in both cell lines and primary tumors, suggesting that these states are pathologically relevant. These findings also challenge the canonical view that cyclin D1 is promoting the expression of cyclin E by derepressing E2F, which is one of the central precepts of the classical CDK4/6-RB pathway. From these relationships, it is possible to develop classifiers using logistic regression that are accurate in predicting the sensitivity to palbociclib. Such tools as shown here could be important in defining tumors with little or no benefit from CDK4/6 inhibitors, which remains a significant clinical issue (Anurag et al., 2020).

Targeting the cell cycle has emerged as a clinically significant regimen. However, as shown here, cell-cycle diversity and adaptations can limit the success of such approaches. Taking into consideration different cell-cycle states, we were able to identify genes and drugs that had a degree of selectivity. Gene networks indicate that different cell-cycle states are more dependent on specific functions. For example, CCNE1 high tumors are more sensitive to the depletion of DNA replication factors, PRC complex, and multiple additional epigenetic factors (e.g., CHAF1, EP300). These findings support potential vulnerabilities and avenues to treat such cancers. In contrast, CCND1 high tumors harbored vulnerabilities to metabolic genes (e.g., PGK1, ENO1) and other processes that could be similarly targeted or used in combination with CDK4/6 or other cytostatic agents. We also uncovered highly unexpected relationships, such as that CDKN2A high tumors exhibited vulnerability to TP53 depletion, which suggests a dependence of these tumor cells on the gain-of-function activity of mutant TP53. This finding is consistent with CDKN2A high cells being particularly resistant to MDM2/4 inhibitors. A feature of these analyses is that it would appear that fundamentally, high CCND1/RB1 and high CCNE1/CDKN2A tumors need to be treated differently. Cytostatic-acting therapies, notably MEK and CDK4/6 inhibitors, act selectively in CCND1/RB1 high tumors, and RB-deficient tumors remain resistant to not only single agent but also combination strategies, as observed in xenograft studies. In CCNE1/CDKN2A high tumors, cytotoxic agents that target the cell cycle (particularly WEE1 inhibitors) are more effective. In addition, it would appear that such tumors are primed toward apoptosis, as indicated by the increased sensitivity to Survivin and BCL2 inhibitors. This adds to an expanding literature that there are collateral vulnerabilities associated with cell-cycle deregulation or survival pathways that have been most studied in the context of RB loss (Gong et al., 2018; Oser et al., 2018; Pearson et al., 2021; Witkiewicz et al., 2018). Given the universal requirement for some of these genes, using combinations it is possible to expand the therapeutic window and increase the selectivity for RB deficiency, as we show using isogenic models. Expanded analyses of these synergistic combinatorial approaches illustrate that the enhanced cell-cycle-specific targeted therapies can be used in tumor models (data not shown). Together, these data suggest that the intrinsically different cell-

cycle states define tumors that should be treated in a distinct fashion with combinatorial strategies that expand upon cell-cycle dependencies and collateral vulnerabilities.

Limitations of the study

The data presented here emerged from the analyses of large publicly available datasets and biochemical functional analyses from a limited number of breast cancer cell lines. Further analyses will be required to determine the breadth of these findings in additional models and tumor types. Of particular importance will be determining whether normal cells that represent the cell of origin of a specific tumor type are in fact using these mechanisms for G1/S control or whether they are solely cancer specific. Another feature that remains under analysis is the potential need to target multiple cyclin or CDK genes in parallel to halt cell-cycle progression. We consider that this will be necessary to understand highly discordant cell cycles, as exemplified by the MB-468 cell line here.

To fully develop gene expression determinants associated with the response to CDK4/6 inhibitors will require the utilization of patient cohorts. This represents a challenge as few patients are treated with CDK4/6 inhibitors as single agents, as assessed in the preclinical models described here. The cell-cycle states that are differentially defined by CCND1/RB or CCNE1/CDKN2A could be considerably more complex and conditioned by the contexts in which these genes are amplified or deleted. More study within a given tumor type and with the use of isogenic lines will be required to fully credential the genetic and therapeutic dependencies that are uncovered here. Furthermore, combination treatments that are particularly effective against RB-deficient or cyclin E-driven models will need to be validated *in vivo* and across more models to determine potential clinical validity.

STAR★METHODS

RESOURCE AVAILABILITY

Lead contact—Further information and requests for resources and reagents should be directed to and will be fulfilled by the lead contact, Erik Knudsen (erik.knudsen@roswellpark.org)

Materials availability—All unique/stable reagents generated in this study are available from the Lead Contact with a completed Materials Transfer Agreement

Data and code availability

- This paper analyzes existing, publicly available data, links to the datasets used are listed in the key resources table. All other data reported in this paper will be shared by the lead contact upon request.
- The paper does not report original code.
- Any additional information required to reanalyze the data reported in this paper is available from the lead author upon request.

EXPERIMENTAL MODELS AND SUBJECT DETAILS

Public cell line and clinical data—The DepMap data and the cell line RNA seq, mutation, copy number, and sample information were obtained from the depmap data portal (https://depmap.org/portal/download/) consisting of 1811 cell lines from 35 distinct cancer types. All the TCGA datasets were acquired from cBioportal from the PanCancer Atlas Study (https://www.cbioportal.org/datasets). These data consist of 31 tumor types.

Cell lines—Different TNBC cell lines, HCC1806, MB-436 and MB-468 were grown in RPMI media containing 10% FBS. MCF7 and MB231 cells were cultured in DMEM medium containing 10% FBS. The MB-157 cell line was cultured in Mcoy5 medium supplemented with 10% FBS. All the cells lines were grown at 37°C and 5% CO_2 and were confirmed to be mycoplasma free. Cell-line authentication were performed using STR analysis.

***In vivo* PDX studies—**Human female breast cancer samples (average age 54) were collected and studied under approved IRB protocols #89989 and #10924 at Huntsman Cancer Institute, University of Utah that obtained patient consent. The University of Utah Institutional Animal Care and Use Committee (IACUC) approved all procedures using live animals. Tumors were implanted at the age of 3–4 weeks. All animals were housed under standard, regulated conditions: food and water given ad lib; housing temperature range 68 – 79 degrees humidity range: 30 – 70%; and a 12 hour light cycle (6am-6pm = On, 6pm-6am = Off). Cryopreserved tumor fragments were implanted into the inguinal mammary fat pad of female NSG mice (n = 20 mice per PDX cohort) using previously described methods (DeRose et al., 2013). When tumors reached 100–150 mm^3, mice with similarly sized tumors were randomized to treatment groups (3–7 mice per group). AZD8186 (reconstituted in corn oil) was given at a dose of 30 mg/kg, oral, twice per day (4 days on, 3 days off). Palbociclib (reconstituted in 50mM sodium lactate) was given at a dose of 100 mg/kg, oral, once per day (5 days on, 2 days off). Combinations used the same dose and schedule as the single agents. Mice were treated for a 21-day period, and tumors were measured using calipers.

TNBC clinical samples—Study cases were obtained from surgical pathology files at Thomas Jefferson University with Institutional Review Board approval and patient consent. All cases are from female breast cancer with an average age of 55 and have been previously described (Adams et al., 2018). Evaluable primary TNBC tumors (n=149) were available in a TMA format.

METHOD DETAILS

Clustering of cancer cell lines based on dependancy—Cancer cell lines were clustered based on their dependency for CDK and CCN genes using k-means clustering in R to give 6 distinct clusters. The alteration of these clusters where represented using the oncoprint package in R. The Pearson’s chi square test in R was used to show the statistical difference in alteration between clusters for each gene. Odds ratios defined in R were used to find the significance of a cancer type occurring in a particular cluster.

Enrichment analyses—Enrichment of cancer cell lines of each tumor types based on the dependency score for CCN and CDK genes were calculated using fgsea package in R. The fgsea function uses a list of cancer types along with the cell lines associated with that cancer type and a table containing information regarding the dependency score of cell lines for each gene to calculate enrichment. Conventional Gene Set Enrichment Analysis (GSEA) was performed using GSEA version 4.1.0. Briefly, gene name and $\log_2$ FoldChange columns were extracted from the output files of deferential gene expression analysis using DESeq2 to serve as the Ranked List (.rnk) files. Four .rnk files were generated using DESeq2 output files between the pair-wise contrasts (cluster1 vs. cluster3; cluster1 vs. cluster4; cluster2 vs. cluster 3 and cluster2 vs. cluster4). Each of these files was used as Ranked List file for the tool ‘‘Run GSEAPreranked’’. The parameters we used to run this tool are as follows: Gene sets database: ftp.broadinstitute.org://pub/gsea/gene_sets/h.all.v7.4.symbols.gmt; Number of permutations: 1000; Collapse/Remap to gene symbols: No_Collapse; Chip platform: ftp.broadinstitute.org://pub/gsea/annotations_versioned/Human_Gene_Symbol_with_Remapping_MSigDB.v7.4.chip.

Logistic regression to predict dependency—The log fold change and the p-value were calculated using a standard two tailed student t-test between gene expression of cell lines belonging to cluster(m) Vs cluster(n) (where m,n=1,2,3,4,5,6 and m≠n). A cutoff of +0.5 and −0.5 for log fold change and 0.05 for p-value were used to extract differentially expressed genes and illustrated in volcano plots. Based on the dependency score of CDK and CCN family genes, cell lines where classified as resistant (those cell lines who’s dependency score is greater than the 25th percentile dependency score) or vulnerable (those cell lines who’s dependency score is lesser than the 25th percentile dependency score). The gene expression of top 10 expressed genes in cluster(m) and top 10 expressed genes in cluster(n) from the volcano plot between cluster(m) Vs cluster(n) (where m,n=1,2,3,4,5,6 and m≠n) was used to predict if a cell line is resistant or vulnerable to a gene G (where G are genes belonging to the CCN and CDK family) using logistic regression. Stepwise algorithm was used to remove unimportant genes that do not contribute significantly in the prediction of sensitivity. In order to test the accuracy of the Logistic regression model the data is divided into 2 sets: a) Training set which accounts to 2/3^{rds} of the data. This consists of gene expression of genes used as dependent variables to predict if the cell line is resistant or vulnerable. The training set is used to create alogistic regression model based on Cluster(m) vs Cluster(n) to predict sensitivity/resistants of gene G for each cell line. b) Test set which accounts to 1/3rd of the data. This consists of gene expression of genes used as dependent variables. The test set is used to test the validity of the model. The accuracy of the model is tested on the test set by constructing an ROC curve showing sensitivity and specificity of the model. The model was also used to predict vulnerability/resistant of breast cancer and ovarian cancer cell lines based on IC50 values (1000 nM is used as cutoff with IC50 value<1000n as sensitive and IC50>1000nm as resistant) of palbociclib.

Therapeutic agents, plasmids and infection procedures—Palbociclib (IBRANCE) was purchased from MedChemExpress (NJ, USA). AZD8186 (S7694), YM155 (S1130), Alisertib (S1133), Pemetrexed (S1135), Navitoclax (S1001) were purchased from Sellckchem (Houston, TX). All drugs were dissolved in DMSO for cell culture use. CSII-

EF lentiviral vector containing the cDNA for HDHB fused to mCHERRY was from Dr. Spencer's laboratory (Gookin et al., 2017). Lentiviral infection was performed on H2B-GFP labelled MB436 and MB468 cells. The translocation of HDHB between cytoplasm and nucleus was captured using IncuCyte imaging.

Cell proliferation assays and toxicity—Select cultures were transduced to stably express H2B-GFP as an independent measure for proliferation. The GFP positive cells were selected using using BD FACSAria II cell sorter. The proliferation of the H2B-GFP cell lines was determined using IncuCyte live-cell imaging systems. The cell counts were determined based on the number of GFP-labelled nuclei and the data were exported to GraphPad Prism for statistical analysis and graph generation. The cell-cycle progression was determined using a chemiluminescent ELISA BrdU incorporation assay (Sigma; 11669915001) following the manufacturer's protocol. Luminescence was read on a BioTEK Synergy 2 plate reader. Each drug treatment was performed in triplicates and confirmed in two independent experiments.

Knockdown experiments—Cells were reverse transfected with gene specific siRNAs using Dharmacon Human On-target plus siRNA: CDK4 (L-003238–00-0005), CDK6 (L-003240–00-0005), Cyclin D1 (L-003210–00-0005) Cyclin E1 (L-003213–00-0005), Cyclin A (L-003205–00-0005), CDKN1B (L-003472–00-0005), CDK2 (L-003236–00-0005), and non-targeting siRNA (D-001810–10-05). CDK2 siRNA (ID# 103569) was purchased from Thermo Fisher. Transfection was performed using Lipofectamine RNAiMax Transfection Reagent (Invitrogen, 13778150). Following 24 H transfection cells were treated with palbociclib or DMSO. The transfection efficiency of the siRNAs was determined by western blotting.

Immunoblot analysis—Whole cell extracts were prepared using RIPA lysis buffer (10 mM Tris HCl, pH 8.0, 1mM EDTA, 150 mM NaCl, 1% Triton-X-100, 0.1% sodium deoxycholate, 0.1% SDS) in the presence of 1X Halt protease inhibitor (Thermo Fisher) and 1 mM PMSF (Sigma, St Louis, MA). The resulting proteins were resolved on an SDS-PAGE gel and the proteins were then transferred to nitro-cellulose membrane for immune blotting. The membranes were incubated with protein-specific primary antibodies overnight at 4°C followed by incubation with HRP-tagged anti-mouse or anti-rabbit secondary antibodies for 1 hour at room temperature. An enhanced chemiluminescence kit (Thermo Fisher, Waltham, MA) was used to detect the immuno-reactive bands. The primary antibodies purchased from Cell-Signaling Technology (Danvers, MA) include pRB S807/811 (8516S), pRB (S780) (9307S), RB-4H1 (9309S), RBL2 (13610S), CDK2 (2546S), CDK4 (12790S), CDK6 (3136S), Cyclin E1 (4129S), P27KIP1 (3686S), and Cyclin B1 (12231S). Phospho-p130 (S672) (Ab76255) was purchased from Abcam. Cyclin D1 (SC20044), Cyclin A (SC271682), CDK1 (SC-54), β Actin (SC47778) and GAPDH (SC-47724) were purchased from Santacruz Biotech, Dallas, TX. Mouse-IgG_k-HRP (Santacruz; SC516102) and Goat-anti-rabbit-HRP (Thermo Fisher; 31460) were used as secondary antibodies. An enhanced chemiluminescent substrate (National Diagnostics; CL-300) was used to detect the immunoreactive bands.

Immunoprecipitation—Total proteins were extracted using the IP-lysis buffer (20 mM Tris-HCl, pH 8.0, 2mM EDTA, 137 mM NaCl, 1% NP-40) in the presence of 1X Halt protease inhibitor (Thermo Fisher) and 1 mM PMSF (Sigma, St Louis, MA). In total, 0.5–0.8 mg of protein from the lysates were incubated with 5 μg of bait antibodies, anti-P27KIP1 (Cell Signaling; 3686S) and anti-Cyclin D1 antibody (Invitrogen: MA5–12707) overnight at 4°C. Mouse (Cell Signaling, 5415S) or rabbit (Cell Signaling, 3900S) IgG1 isotype control was used. Protein immunocomplexes were then incubated with Protein G-agarose or protein A-agarose (Thermo Fisher) at 4°C up to 4H and were then washed 3 times with IP wash buffer (20 mM Tris-HCl, pH 8.0, 100 mM NaCl, 0,5% NP-40). Complex bound to the protein beads were eluted using 2X SDS buffer and were subjected to western blotting.

***In vitro* kinase reactions—**CDK2 and cyclin D1 associated kinase reactions were performed as described in our previous study (Functional determinant). Protein extracts were prepared using kinase lysis buffer (50 mM Tris-HCl pH 7.5, 150 mM NaCl, 0.1% NP-40, 10 mM DTT, 10% glycerol) in the presence of protease inhibitors. Anti-cyclin D1 antibody (Invitrogen: MA5–12707) was used to immunoprecipitate cyclin D1 and its associated CDKs. The kinase reactions were performed using the specific buffer containing 50 mM HEPES-KOH, pH 7.5, 20 mM $MgCl_2$, 1mM DTT in the presence of 2mM ATP. Recombinant RB C-terminal (10μg) was used as a substrate (Knudsen ES, Differential reglation).

To determine CDK2 kinase activity, cells were lysed using CDK2 kinase lysis buffer (50 mM HEPES-KOH pH7.5, 150 mM NaCl, 1 mM EDTA, 1 mM DTT, 0.1% Tween-20). CDK2 complexes were immunoprecipitated using anti-CDK2 antibody (Santacruz; SC-6248). Kinase reactions were carried out in the reaction buffer (40 mM Tris-HCl pH 8, 20 mM $MgCl_2$, 0.1 mg/mL BSA, 50 μM DTT).

Multiplexed IF staining—Formalin-fixed Paraffin-embedded (FFPE) tissue sections orTMAs were cut at 4–5 μm on charged slides. Slides were dried at 65°C for 6 hours. After drying, the slides were placed on the BOND RXm Research Stainer (Leica Biosystems) and deparaffinized with BOND Dewax solution (AR9222, Lecia Biosystems). The multispectral immunofluorescent (mIF) staining process involved serial applications of the following for each biomarker: epitope retrieval/stripping with ER1 (citrate buffer pH 6, AR996, Leica Biosystems), blocking buffer (AKOYA Biosciences), primary antibody, Opal Polymer HRP secondary antibody (AKOYA Biosciences), Opal Fluorophore (AKOYA Biosciences). All AKOYA reagents used for mIF staining come as a kit (NEL821001KT). Spectral DAPI (AKOYA Biosciences) was applied once slides were removed from the BOND. They were cover slipped using an aqueous method and Diamond antifade mounting medium (Invitrogen ThermoFisher). The mIF panel consisted of the following antibodies (clone, company, and opal fluorophores): Cyclin D (SP4, Epredia, Opal 570), Cyclin E (EP435E, abcam, Opal 520), MCM2 (RBT-MCM2, Biosb, Opal Polaris 480), Pan Cytokeratin (AE1AE3, Agilent DAKO, Opal Polaris 780), pHH3 (Ser10, Millipore Sigma, Opal 620), pRB (Ser807/811, Cell Signaling, Opal 690).

Tissue imaging and analysis—Slides were imaged on the Vectra® Polaris Automated Quantitative Pathology Imaging System (AKOYA Biosciences). Further analysis of the

slides was performed using inForm® Software v2.4.11 (AKOYA Biosciences). Whole slide spectral unmixing was achieved using the synthetic spectral library within inForm. From the unmixed images representative cores were selected under the guidance of Dr. Witkiewicz, pathologist, to train tissue and cell segmentation. Next a unique algorithm was created using a machine learning technique, in which the operator selects positive and negative cell examples for each biomarker. These algorithms were then batch applied across the entire TMA. A final quality control review discarded cores with insufficient staining or absence of tumor compartment. The percentage of markers (Cyclin E, Cyclin D1 and pRB) for each core (red: RBpos and blue:RBneg) was calculated and normalized. K-means clustering was applied to the data to generate four clusters.

Breast cancer cell line oncoprint—Data from CCLE was aggregated for breast cancer models used in previous analysis to determine which models had single nucleotide variations (SNVs), insertions/deletions (INDEL), or homozygous deletions (HOMO DEL) or amplifications (AMP). Copy number deletions and amplifications were determined using cutoffs of 0.5 and 1.5, respectively. Mutations for PIK3CA, TP53, PTEN, RB1, and CDKN2A were double checked against ATCC's cell lines by mutation packet. Four missing INDELs were identified and adjusted in the oncoprint (HCC1187: TP53 INDEL, HCC1395: PTEN INDEL, BT549: RB1 INDEL, MDAMB436: RB1 INDEL). Oncoprint was generated using the ComplexHeatmap package in R.

Tissue correlation plot from TCGA—For selected tissue types, the correlation plot for selected TCGA tissue types was generated using the corrplot package in R.

Cell line expression Sankey plot—For cell lines included in K-means analysis from Figure 1 (excluding liquid tumors from cluster 5), CCLE expression data was used to determine cell line groups with high (cell lines in upper 25% of gene expression range), low (lower 25%) and intermediate expression levels for CCND1, CCNE1, RB1 and CDKN2A. Plot was generated using networkD3 in R to compare high/low/intermediate expression groups between genes. Transition lines were colored to reflect the cell lines' expression quantile in CCND1.

Cyclin and RB networks and Sankey plots—For each network and Sankey plot, genes were filtered to exclude genes that had indeterminate vulnerability in either gene (CCND1/CCNE1, RB1/CDKN2A). These genes were then aligned to a protein-protein interaction network downloaded from Biogrid (Homo sapiens, v. 3.5.168) (Oughtred et al., 2021). Only genes with edges to other included genes were kept. Networks were visualized and clustered using Cytoscape. Enrichments were performed using list.to.go from the ALPACA package in R. Sankey plots were generated to show movement of genes between high/low groups using network D3 in R.

Concordance drug analysis, volcano plots + trend lines and p-values—Using the cell line quantile high/low cutoffs in the CCLE expression data (excluding liquid tumors from cluster 5) and the secondary drug screen data from DepMap, drug response log fold changes (logFCs) were calculated between high and low expression cell line groups, using mean response from each group. P-values between high and low groups were determined

using a Student's t-test. LogFCs were then compared across all four genes (CCND1, RB1, CCNE1, CDKN2A) to see which drugs had similar response patterns between high and low expression groups in respective gene pairs (logFC values with the same sign in either CCND1 and RB1, or CDKN2A and CCNE1). These drugs were then filtered to drugs with at least 2 significant p-values across the 4 genes. Only drugs that had multiple doses in the remaining list and at least one logFC greater than +/− 0.2 were shown. Heatmap was generated using the ComplexHeatmap package in R (Gu et al., 2016)

QUANTIFICATION AND STATISTICAL ANALYSIS

Statistical analyses of the data was performed using the methods as described in the ''method details'' in the following sections: Clustering of cancer cell lines based on dependency; Logistic regression to predict dependency; Tissue imaging and analysis; Concordance drug analysis, volcano plots + trend lines and p-values. The exact number of animals for PDX studies is provided in the figures. The number of replicates and measures of significance are present in the figure legends and denoted in the figures.

Supplementary Material

Refer to Web version on PubMed Central for supplementary material.

ACKNOWLEDGMENTS

The authors would like to thank their colleagues for thought-provoking conversations and editing. The research reported on the TNBC PDX models used the Preclinical Research Shared Resource at Huntsman Cancer Institute at the University of Utah and was supported by the National Cancer Institute of the National Institutes of Health under award no. P30CA042014 (to A.L.W.). Mutlispectral imaging was performed in the Advanced Tissue Analyses Shared Resource at Roswell Park that is supported by National Cancer Institute grant P30CA016056. Other funding was provided by NIH/NCI R01 CA247362 and CA211878 (to E.S.K. and A.K.W.).

REFERENCES

Adams TA, Vail PJ, Ruiz A, Mollaee M, McCue PA, Knudsen ES, and Witkiewicz AK (2018). Composite analysis of immunological and metabolic markers defines novel subtypes of triple negative breast cancer. Mod. Pathol 31, 288–298. 10.1038/modpathol.2017.126. [PubMed: 28984302]

Alvarez-Fernandez M, and Malumbres M (2020). Mechanisms of sensitivity and resistance to CDK4/6 inhibition. Cancer Cell 37, 514–529. 10.1016/j.ccell.2020.03.010. [PubMed: 32289274]

Anurag M, Haricharan S, and Ellis MJ (2020). CDK4/6 inhibitor biomarker Research: are we barking up the wrong tree? Clin. Cancer Res 26, 3–5. 10.1158/1078-0432.CCR-19-3119. [PubMed: 31690650]

Asghar U, Witkiewicz AK, Turner NC, and Knudsen ES (2015). The history and future of targeting cyclin-dependent kinases in cancer therapy. Nat. Rev. Drug Discov 14, 130–146. 10.1038/nrd4504. [PubMed: 25633797]

Barriere C, Santamaria D, Cerqueira A, Galan J, Martin A, Ortega S, Malumbres M, Dubus P, and Barbacid M (2007). Mice thrive without Cdk4 and Cdk2. Mol. Oncol 1, 72–83. 10.1016/j.molonc.2007.03.001. [PubMed: 19383288]

Bartkova J, Rezaei N, Liontos M, Karakaidos P, Kletsas D, Issaeva N, Vassiliou LV, Kolettas E, Niforou K, Zoumpourlis VC, et al. (2006). Oncogene-induced senescence is part of the tumorigenesis barrier imposed by DNA damage checkpoints. Nature 444, 633–637. [PubMed: 17136093]

Bertucci F, Ng CKY, Patsouris A, Droin N, Piscuoglio S, Carbuccia N, Soria JC, Dien AT, Adnani Y, Kamal M, et al. (2019). Genomic characterization of metastatic breast cancers. Nature 569, 560–564. 10.1038/s41586-019-1056-z. [PubMed: 31118521]

Burkhart DL, and Sage J (2008). Cellular mechanisms of tumour suppression by the retinoblastoma gene. Nat. Rev. Cancer 8, 671–682. 10.1038/nrc2399. [PubMed: 18650841]

Coverley D, Laman H, and Laskey RA (2002). Distinct roles for cyclins E and A during DNA replication complex assembly and activation. Nat. Cell Biol 4, 523–528. [PubMed: 12080347]

Dean JL, Thangavel C, McClendon AK, Reed CA, and Knudsen ES (2010). Therapeutic CDK4/6 inhibition in breast cancer: key mechanisms of response and failure. Oncogene 29, 4018–4032. 10.1038/onc.2010.154. [PubMed: 20473330]

DeGregori J, Kowalik T, and Nevins JR (1995). Cellular targets for activation by the E2F1 transcription factor include DNA synthesis- and G1/S-regulatory genes. Mol. Cell Biol 15, 4215–4224. [PubMed: 7623816]

DeRose YS, Gligorich KM, Wang G, Georgelas A, Bowman P, Courdy SJ, Welm AL, and Welm BE (2013). Patient-derived models of human breast cancer: protocols for in vitro and in vivo applications in tumor biology and translational medicine. Curr. Protoc. Pharmacol 14, Unit14 23. 10.1002/0471141755.ph1423s60. [PubMed: 23456611]

DeRose YS, Wang G, Lin YC, Bernard PS, Buys SS, Ebbert MT, Factor R, Matsen C, Milash BA, Nelson E, et al. (2011). Tumor grafts derived from women with breast cancer authentically reflect tumor pathology, growth, metastasis and disease outcomes. Nat. Med 17, 1514–1520. 10.1038/nm.2454. [PubMed: 22019887]

Diehl JA (2002). Cycling to cancer with cyclin D1. Cancer Biol. Ther 1, 226–231. [PubMed: 12432268]

Diril MK, Ratnacaram CK, Padmakumar VC, Du T, Wasser M, Coppola V, Tessarollo L, and Kaldis P (2012). Cyclin-dependent kinase 1 (Cdk1) is essential for cell division and suppression of DNA re-replication but not for liver regeneration. Proc. Natl. Acad. Sci. U S A 109, 3826–3831. 10.1073/pnas.1115201109. [PubMed: 22355113]

Finn RS, Dering J, Conklin D, Kalous O, Cohen DJ, Desai AJ, Ginther C, Atefi M, Chen I, Fowst C, et al. (2009). PD 0332991, a selective cyclin D kinase 4/6 inhibitor, preferentially inhibits proliferation of luminal estrogen receptor-positive human breast cancer cell lines in vitro. Breast Cancer Res 11, R77. 10.1186/bcr2419. [PubMed: 19874578]

Gao H, Korn JM, Ferretti S, Monahan JE, Wang Y, Singh M, Zhang C, Schnell C, Yang G, Zhang Y, et al. (2015). High-throughput screening using patient-derived tumor xenografts to predict clinical trial drug response. Nat. Med 21, 1318–1325. 10.1038/nm.3954. [PubMed: 26479923]

Goel S, DeCristo MJ, McAllister SS, and Zhao JJ (2018). CDK4/6 inhibition in cancer: beyond cell cycle arrest. Trends Cell Biol 28, 911–925. 10.1016/j.tcb.2018.07.002. [PubMed: 30061045]

Gong X, Du J, Parsons SH, Merzoug FF, Webster Y, Iversen PW, Chio LC, Van Horn RD, Lin X, Blosser W, et al. (2018). Aurora-A kinase inhibition is synthetic lethal with loss of the RB1 tumor suppressor gene. Cancer Discov 9, 248–263. 10.1158/2159-8290.CD-18-0469. [PubMed: 30373917]

Goodwin EC, and DiMaio D (2000). Repression of human papillomavirus oncogenes in HeLa cervical carcinoma cells causes the orderly reactivation of dormant tumor suppressor pathways. Proc. Natl. Acad. Sci. U S A 97, 12513–12518. 10.1073/pnas.97.23.12513. [PubMed: 11070078]

Gookin S, Min M, Phadke H, Chung M, Moser J, Miller I, Carter D, and Spencer SL (2017). A map of protein dynamics during cell-cycle progression and cell-cycle exit. PLoS Biol 15, e2003268. 10.1371/journal.pbio.2003268. [PubMed: 28892491]

Gopinathan L, Tan SL, Padmakumar VC, Coppola V, Tessarollo L, and Kaldis P (2014). Loss of Cdk2 and cyclin A2 impairs cell proliferation and tumorigenesis. Cancer Res 74, 3870–3879. 10.1158/0008-5472.CAN-13-3440. [PubMed: 24802190]

Gu Z, Eils R, and Schlesner M (2016). Complex heatmaps reveal patterns and correlations in multidimensional genomic data. Bioinformatics 32, 2847– 2849. 10.1093/bioinformatics/btw313. [PubMed: 27207943]

Hartwell LH, and Kastan MB (1994). Cell cycle control and cancer. Science 266, 1821–1828. 10.1126/science.7997877. [PubMed: 7997877]

Herrera-Abreu MT, Palafox M, Asghar U, Rivas MA, Cutts RJ, Garcia-Murillas I, Pearson A, Guzman M, Rodriguez O, Grueso J, et al. (2016). Early adaptation and acquired resistance to CDK4/6 inhibition in estrogen receptor-positive breast cancer. Cancer Res 76, 2301–2313. 10.1158/0008-5472.CAN-15-0728. [PubMed: 27020857]

Hinds PW, Mittnacht S, Dulic V, Arnold A, Reed SI, and Weinberg RA (1992). Regulation of retinoblastoma protein functions by ectopic expression of human cyclins. Cell 70, 993–1006. [PubMed: 1388095]

Johnson DG, and Schneider-Broussard R (1998). Role of E2F in cell cycle control and cancer. Front Biosci 3, D447–D448. [PubMed: 9556498]

Jones RM, Mortusewicz O, Afzal I, Lorvellec M, Garcia P, Helleday T, and Petermann E (2013). Increased replication initiation and conflicts with transcription underlie Cyclin E-induced replication stress. Oncogene 32, 3744–3753. 10.1038/onc.2012.387. [PubMed: 22945645]

Kalaszczynska I, Geng Y, Iino T, Mizuno S, Choi Y, Kondratiuk I, Silver DP, Wolgemuth DJ, Akashi K, and Sicinski P (2009). Cyclin A is redundant in fibroblasts but essential in hematopoietic and embryonic stem cells. Cell 138, 352–365. 10.1016/j.cell.2009.04.062. [PubMed: 19592082]

Knudsen ES, Pruitt SC, Hershberger PA, Witkiewicz AK, and Goodrich DW (2019). Cell cycle and beyond: exploiting new RB1 controlled mechanisms for cancer therapy. Trends Cancer 5, 308–324. 10.1016/j.trecan.2019.03.005. [PubMed: 31174843]

Knudsen ES, and Witkiewicz AK (2016). Defining the transcriptional and biological response to CDK4/6 inhibition in relation to ER+/HER2-breast cancer. Oncotarget 7, 69111–69123. 10.18632/oncotarget.11588. [PubMed: 27564114]

Knudsen ES, and Witkiewicz AK (2017). The strange case of CDK4/6 inhibitors: mechanisms, resistance, and combination strategies. Trends Cancer 3, 39–55. 10.1016/j.trecan.2016.11.006. [PubMed: 28303264]

Knudsen KE, Fribourg AF, Strobeck MW, Blanchard JM, and Knudsen ES (1999). Cyclin A is a functional target of retinoblastoma tumor suppressor protein-mediated cell cycle arrest. J. Biol. Chem 274, 27632–27641. [PubMed: 10488103]

Konecny GE, Winterhoff B, Kolarova T, Qi J, Manivong K, Dering J, Yang G, Chalukya M, Wang HJ, Anderson L, et al. (2011). Expression of p16 and retinoblastoma determines response to CDK4/6 inhibition in ovarian cancer. Clin. Cancer Res 17, 1591–1602. 10.1158/1078-0432.CCR-10-2307. [PubMed: 21278246]

Kozar K, Ciemerych MA, Rebel VI, Shigematsu H, Zagozdzon A, Sicinska E, Geng Y, Yu Q, Bhattacharya S, Bronson RT, et al. (2004). Mouse development and cell proliferation in the absence of D-cyclins. Cell 118, 477–491. 10.1016/j.cell.2004.07.025. [PubMed: 15315760]

Kumarasamy V, Vail P, Nambiar R, Witkiewicz AK, and Knudsen ES (2020). Functional determinants of cell-cycle plasticity and sensitivity to CDK4/6 inhibition. Cancer Res 81, 1347–1360. 10.1158/0008-5472.CAN-20-2275. [PubMed: 33323381]

Lam EW, Glassford J, Banerji L, Thomas NS, Sicinski P, and Klaus GG (2000). Cyclin D3 compensates for loss of cyclin D2 in mouse B-lymphocytes activated via the antigen receptor and CD40. J. Biol. Chem 275, 3479– 3484. [PubMed: 10652342]

Leng X, Connell-Crowley L, Goodrich D, and Harper JW (1997). S-Phase entry upon ectopic expression of G1 cyclin-dependent kinases in the absence of retinoblastoma protein phosphorylation. Curr. Biol 7, 709–712. [PubMed: 9285720]

Li Z, Razavi P, Li Q, Toy W, Liu B, Ping C, Hsieh W, Sanchez-Vega F, Brown DN, Da Cruz Paula AF, et al. (2018). Loss of the FAT1 tumor suppressor promotes resistance to CDK4/6 inhibitors via the hippo pathway. Cancer Cell 34, 893–905 e898. 10.1016/j.ccell.2018.11.006. [PubMed: 30537512]

Ludlow JW, and Skuse GR (1995). Viral oncoprotein binding to pRB, p107, p130, and p300. Virus Res 35, 113–121. 10.1016/0168-1702(94)00094-s. [PubMed: 7762286]

Malumbres M, and Barbacid M (2001). To cycle or not to cycle: a critical decision in cancer. Nat. Rev. Cancer 1, 222–231. [PubMed: 11902577]

Malumbres M, and Barbacid M (2006). Is Cyclin D1-CDK4 kinase a bona fide cancer target? Cancer Cell 9, 2–4. 10.1016/j.ccr.2005.12.026. [PubMed: 16413464]

Malumbres M, Sotillo R, Santamaria D, Galan J, Cerezo A, Ortega S, Dubus P, and Barbacid M (2004). Mammalian cells cycle without the D-type cyclin-dependent kinases Cdk4 and Cdk6. Cell 118, 493–504. 10.1016/j.cell.2004.08.002. [PubMed: 15315761]

McFarland JM, Ho ZV, Kugener G, Dempster JM, Montgomery PG, Bryan JG, Krill-Burger JM, Green TM, Vazquez F, Boehm JS, et al. (2018). Improved estimation of cancer dependencies from large-scale RNAi screens using model-based normalization and data integration. Nat. Commun 9, 4610. 10.1038/s41467-018-06916-5. [PubMed: 30389920]

Narasimha AM, Kaulich M, Shapiro GS, Choi YJ, Sicinski P, and Dowdy SF (2014). Cyclin D activates the Rb tumor suppressor by mono-phosphorylation. Elife 3, e02872. 10.7554/eLife.02872.

Nevins JR (2001). The Rb/E2F pathway and cancer. Hum. Mol. Genet 10, 699–703. [PubMed: 11257102]

Nurse P (2012). Finding CDK: linking yeast with humans. Nat. Cell Biol 14, 776. 10.1038/ncb2547. [PubMed: 22854809]

O'Brien N, Conklin D, Beckmann R, Luo T, Chau K, Thomas J, Mc Nulty A, Marchal C, Kalous O, von Euw E, et al. (2018). Preclinical activity of abemaciclib alone or in combination with antimitotic and targeted therapies in breast cancer. Mol. Cancer Ther 17, 897–907. 10.1158/1535-7163.MCT-17-0290. [PubMed: 29483214]

O'Leary B, Cutts RJ, Liu Y, Hrebien S, Huang X, Fenwick K, Andre F, Loibl S, Loi S, Garcia-Murillas I, et al. (2018a). The genetic landscape and clonal evolution of breast cancer resistance to palbociclib plus fulvestrant in the PALOMA-3 trial. Cancer Discov 8, 1390–1403. 10.1158/2159-8290.CD-18-0264. [PubMed: 30206110]

O'Leary B, Hrebien S, Morden JP, Beaney M, Fribbens C, Huang X, Liu Y, Bartlett CH, Koehler M, Cristofanilli M, et al. (2018b). Early circulating tumor DNA dynamics and clonal selection with palbociclib and fulvestrant for breast cancer. Nat. Commun 9, 896. 10.1038/s41467-018-03215-x. [PubMed: 29497091]

Oser MG, Fonseca R, Chakraborty AA, Brough R, Spektor A, Jennings RB, Flaifel A, Novak JS, Gulati A, Buss E, et al. (2018). Cells lacking the RB1 tumor suppressor gene are hyperdependent on aurora B kinase for survival. Cancer Discov 9, 230–247. 10.1158/2159-8290.CD-18-0389. [PubMed: 30373918]

Oughtred R, Rust J, Chang C, Breitkreutz BJ, Stark C, Willems A, Boucher L, Leung G, Kolas N, Zhang F, et al. (2021). The BioGRID database: a comprehensive biomedical resource of curated protein, genetic, and chemical interactions. Protein Sci 30, 187–200. 10.1002/pro.3978. [PubMed: 33070389]

Pearson JD, Huang K, Pacal M, McCurdy SR, Lu S, Aubry A, Yu T, Wadosky KM, Zhang L, Wang T, et al. (2021). Binary pan-cancer classes with distinct vulnerabilities defined by pro- or anti-cancer YAP/TEAD activity. Cancer Cell 39, 1115–1134.e2. 10.1016/j.ccell.2021.06.016. [PubMed: 34270926]

Pozo K, Castro-Rivera E, Tan C, Plattner F, Schwach G, Siegl V, Meyer D, Guo A, Gundara J, Mettlach G, et al. (2013). The role of Cdk5 in neuroendocrine thyroid cancer. Cancer Cell 24, 499–511. 10.1016/j.ccr.2013.08.027. [PubMed: 24135281]

Rubin SM, Sage J, and Skotheim JM (2020). Integrating old and new paradigms of G1/S control. Mol. Cell 80, 183–192. 10.1016/j.molcel.2020.08.020. [PubMed: 32946743]

Sadasivam S, and DeCaprio JA (2013). The DREAM complex: master coordinator of cell cycle-dependent gene expression. Nat. Rev. Cancer 13, 585–595. 10.1038/nrc3556. [PubMed: 23842645]

Sanidas I, Morris R, Fella KA, Rumde PH, Boukhali M, Tai EC, Ting DT, Lawrence MS, Haas W, and Dyson NJ (2019). A code of mono-phosphorylation modulates the function of RB. Mol. Cell 73, 985–1000 e1006. 10.1016/j.molcel.2019.01.004. [PubMed: 30711375]

Santamaria D, Barriere C, Cerqueira A, Hunt S, Tardy C, Newton K, Caceres JF, Dubus P, Malumbres M, and Barbacid M (2007). Cdk1 is sufficient to drive the mammalian cell cycle. Nature 448, 811–815. 10.1038/nature06046. [PubMed: 17700700]

Scheicher R, Hoelbl-Kovacic A, Bellutti F, Tigan AS, Prchal-Murphy M, Heller G, Schneckenleithner C, Salazar-Roa M, Zochbauer-Muller S, Zuber J, et al. (2015). CDK6 as a key

regulator of hematopoietic and leukemic stem cell activation. Blood 125, 90–101. 10.1182/blood-2014-06-584417. [PubMed: 25342715]

Shapiro GI (2006). Cyclin-dependent kinase pathways as targets for cancer treatment. J. Clin. Oncol 24, 1770–1783. 10.1200/JCO.2005.03.7689. [PubMed: 16603719]

Sherr CJ (1995). D-type cyclins. Trends Biochem. Sci 20, 187–190. [PubMed: 7610482]

Sherr CJ (1996). Cancer cell cycles. Science 274, 1672–1677. [PubMed: 8939849]

Sherr CJ (2000). Cell cycle control and cancer. Harvey Lect 96, 73–92. [PubMed: 12200872]

Sicinska E, Aifantis I, Le Cam L, Swat W, Borowski C, Yu Q, Ferrando AA, Levin SD, Geng Y, von Boehmer H, and Sicinski P (2003). Requirement for cyclin D3 in lymphocyte development and T cell leukemias. Cancer Cell 4, 451–461. [PubMed: 14706337]

Suski JM, Braun M, Strmiska V, and Sicinski P (2021). Targeting cell-cycle machinery in cancer. Cancer Cell 39, 759–778. 10.1016/j.ccell.2021.03.010. [PubMed: 33891890]

Tetsu O, and McCormick F (2003). Proliferation of cancer cells despite CDK2 inhibition. Cancer Cell 3, 233–245. 10.1016/s1535-6108(03)00053-9. [PubMed: 12676582]

Tsherniak A, Vazquez F, Montgomery PG, Weir BA, Kryukov G, Cowley GS, Gill S, Harrington WF, Pantel S, Krill-Burger JM, et al. (2017). Defining a cancer dependency map. Cell 170, 564–576 e516. 10.1016/j.cell.2017.06.010. [PubMed: 28753430]

Turner NC, Liu Y, Zhu Z, Loi S, Colleoni M, Loibl S, DeMichele A, Harbeck N, Andre F, Bayar MA, et al. (2019). Cyclin E1 expression and palbociclib efficacy in previously treated hormone receptor-positive metastatic breast cancer. J. Clin. Oncol 37, 1169–1178. 10.1200/JCO.18.00925. [PubMed: 30807234]

VanArsdale T, Boshoff C, Arndt KT, and Abraham RT (2015). Molecular pathways: targeting the cyclin D-CDK4/6 Axis for cancer treatment. Clin. Cancer Res 21, 2905–2910. 10.1158/1078-0432.CCR-14-0816. [PubMed: 25941111]

Wander SA, Cohen O, Gong X, Johnson GN, Buendia-Buendia JE, Lloyd MR, Kim D, Luo F, Mao P, Helvie K, et al. (2020). The genomic landscape of intrinsic and acquired resistance to cyclin-dependent kinase 4/6 inhibitors in patients with hormone receptor positive metastatic breast cancer. Cancer Discov 10, 1174–1193. 10.1158/2159-8290.CD-19-1390. [PubMed: 32404308]

Weinberg RA (1995). The retinoblastoma protein and cell cycle control. Cell 81, 323–330. [PubMed: 7736585]

Witkiewicz AK, Chung S, Brough R, Vail P, Franco J, Lord CJ, and Knudsen ES (2018). Targeting the vulnerability of RB tumor suppressor loss in triple-negative breast cancer. Cell Rep 22, 1185–1199. 10.1016/j.celrep.2018.01.022. [PubMed: 29386107]

Witkiewicz AK, Knudsen KE, Dicker AP, and Knudsen ES (2011). The meaning of p16(ink4a) expression in tumors: functional significance, clinical associations and future developments. Cell Cycle 10, 2497–2503. [PubMed: 21775818]

Xiong Y, Zhang H, and Beach D (1993). Subunit rearrangement of the cyclin-dependent kinases is associated with cellular transformation. Genes Dev 7, 1572–1583. [PubMed: 8101826]

Highlights

- There is significant heterogeneity in the requirement for G1/S-promoting CDK/cyclins
- Reciprocal expression relationships denote divergent cell-cycle states in tumors
- Specific vulnerabilities are associated with different cell-cycle utilization
- Multiple separable mechanisms drive cell-cycle progression in tumor cells

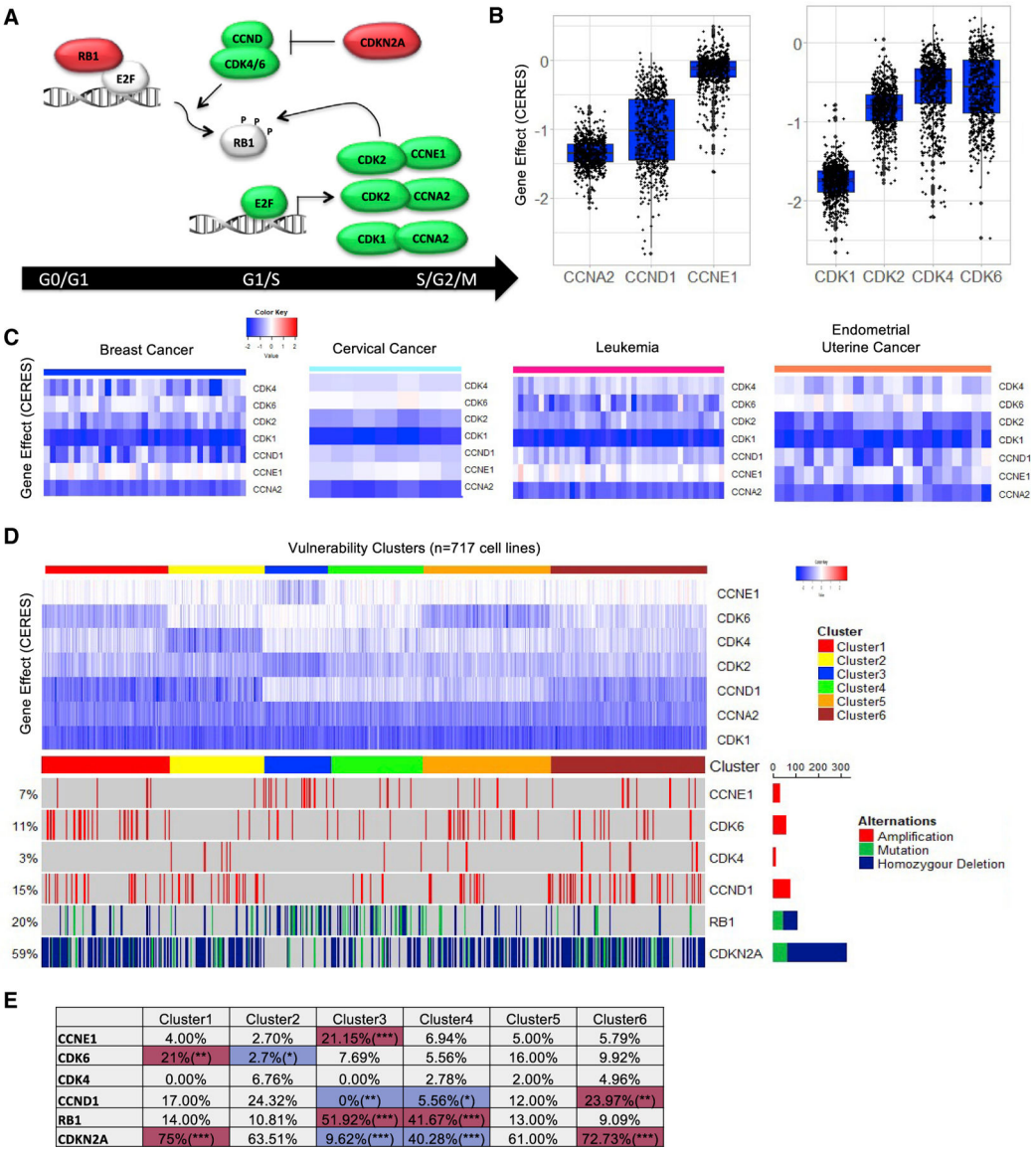

E

	Cluster1	Cluster2	Cluster3	Cluster4	Cluster5	Cluster6
CCNE1	4.00%	2.70%	21.15%(***)	6.94%	5.00%	5.79%
CDK6	21%(**)	2.7%(*)	7.69%	5.56%	16.00%	9.92%
CDK4	0.00%	6.76%	0.00%	2.78%	2.00%	4.96%
CCND1	17.00%	24.32%	0%(**)	5.56%(*)	12.00%	23.97%(**)
RB1	14.00%	10.81%	51.92%(***)	41.67%(***)	13.00%	9.09%
CDKN2A	75%(***)	63.51%	9.62%(***)	40.28%(***)	61.00%	72.73%(***)

Figure 1. Diverse requirements for CDK and cyclins across cancer cell lines

(A) Schematic of cell-cycle progression and CDK/cyclins.

(B) Boxplot showing dependency to select CDK and cyclin gene members in cancer cell lines (n = 717).

(C) Heatmap showing the dependency of CDK and cyclin genes for representative cancer cell types.

(D) Cancer cell lines were clustered based on their dependency for the indicated CDK and CCN family genes using k-means clustering to give 6 distinct clusters.

(E) Genetic information showing amplification of CCNE1, CDK6, CDK4, and CCND1 and homozygous deletion or mutation of RB1 and CDKN2A for the 6 clusters. Pearson's chi square test was used to find the significance of alteration events between each cluster compared with the rest of the clusters (*p < 0.05, **p < 0.01, ***p < 0.001).

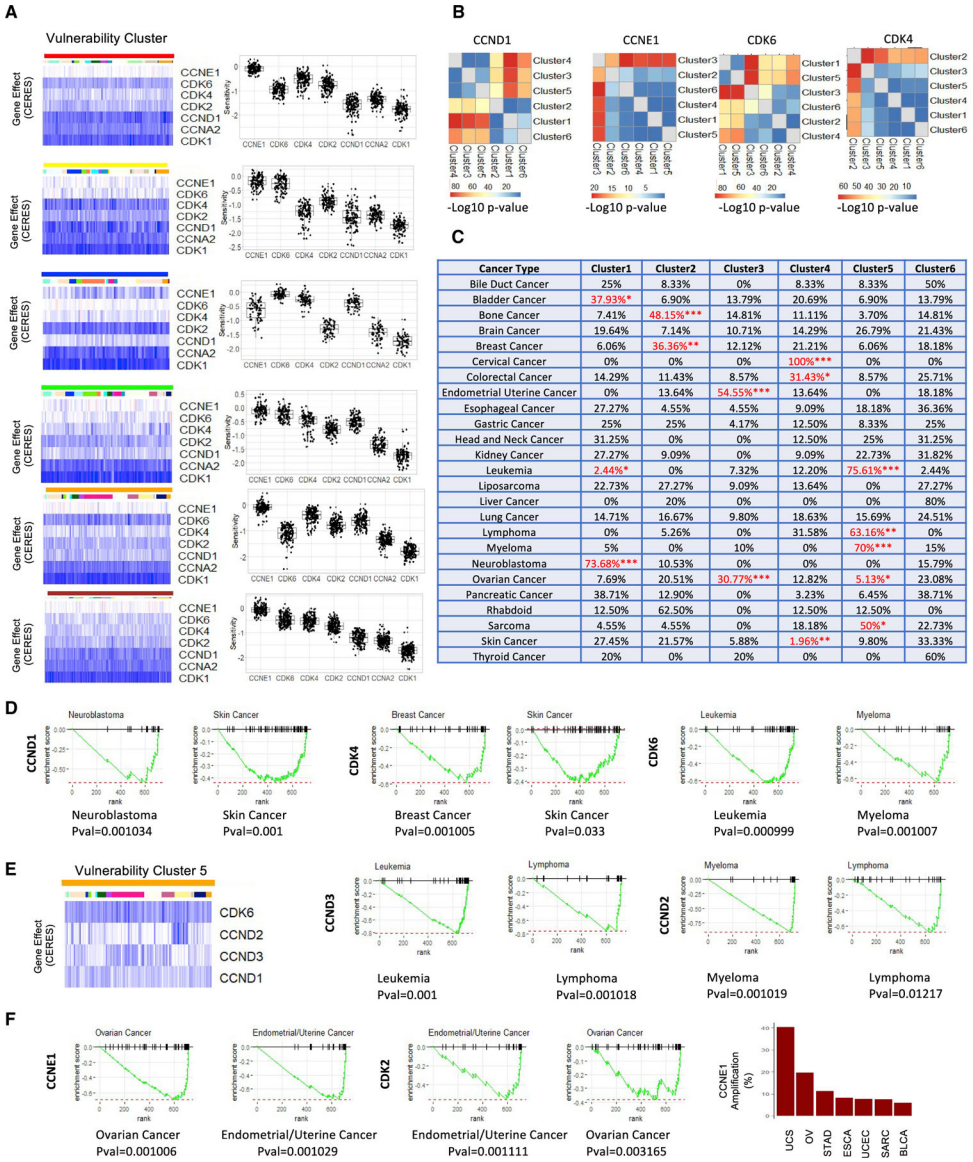

Cancer Type	Cluster1	Cluster2	Cluster3	Cluster4	Cluster5	Cluster6
Bile Duct Cancer	25%	8.33%	0%	8.33%	8.33%	50%
Bladder Cancer	37.93%*	6.90%	13.79%	20.69%	6.90%	13.79%
Bone Cancer	7.41%	48.15%***	14.81%	11.11%	3.70%	14.81%
Brain Cancer	19.64%	7.14%	10.71%	14.29%	26.79%	21.43%
Breast Cancer	6.06%	36.36%**	12.12%	21.21%	6.06%	18.18%
Cervical Cancer	0%	0%	0%	100%***	0%	0%
Colorectal Cancer	14.29%	11.43%	8.57%	31.43%*	8.57%	25.71%
Endometrial Uterine Cancer	0%	13.64%	54.55%***	13.64%	0%	18.18%
Esophageal Cancer	27.27%	4.55%	4.55%	9.09%	18.18%	36.36%
Gastric Cancer	25%	25%	4.17%	12.50%	8.33%	25%
Head and Neck Cancer	31.25%	0%	0%	12.50%	25%	31.25%
Kidney Cancer	27.27%	9.09%	0%	9.09%	22.73%	31.82%
Leukemia	2.44%*	0%	7.32%	12.20%	75.61%***	2.44%
Liposarcoma	22.73%	27.27%	9.09%	13.64%	0%	27.27%
Liver Cancer	0%	20%	0%	0%	0%	80%
Lung Cancer	14.71%	16.67%	9.80%	18.63%	15.69%	24.51%
Lymphoma	0%	5.26%	0%	31.58%	63.16%**	0%
Myeloma	5%	0%	10%	0%	70%***	15%
Neuroblastoma	73.68%***	10.53%	0%	0%	0%	15.79%
Ovarian Cancer	7.69%	20.51%	30.77%***	12.82%	5.13%*	23.08%
Pancreatic Cancer	38.71%	12.90%	0%	3.23%	6.45%	38.71%
Rhabdoid	12.50%	62.50%	0%	12.50%	12.50%	0%
Sarcoma	4.55%	4.55%	0%	18.18%	50%*	22.73%
Skin Cancer	27.45%	21.57%	5.88%	1.96%**	9.80%	33.33%
Thyroid Cancer	20%	0%	20%	0%	0%	60%

Figure 2. Tumor type-selective vulnerability to select CDK and cyclin genes

(A) Sensitivity to individual CDK and cyclin depletion is indicated in the heatmap and boxplots for each of the clusters. The clusters are composed of the following number of cell lines: cluster 1, n = 133; cluster 2, n = 105; cluster 3, n = 68; cluster 4, n = 103; cluster 5, n = 138; and cluster 6, n = 170.

(B) Significance of dependency for CCND1, CCNE1, CDK6, and CDK4 between clusters was determined using a paired Student's t test. The −log10 p value is shown in the heatmaps (red represents highly significant and blue is less significant, as denoted in the color bar).

(C) The percentage of a given cancer cell type belonging to each cluster. The statistical significance of cancer cell lines is based on the odds ratio between the cell lines in cancer type and clusters (*p < 0.05, **p < 0.01, ***p < 0.001).

(D) Enrichment of cancer cell lines in the indicated tumor types based on the dependency scores for CCND1, CDK4, and CDK6. The enrichment analysis and statistical significance was performed using the fgsea package in R.

(E) Select analyses of cluster 5 indicating the requirement for CCND2 and CCND3. Enrichment of cancer cell lines in the indicated tumor types based on the dependency score for CCND2 and CCND3.

(F) Enrichment of cancer cell lines in the indicated tumor types based on the dependency score for CDK2 and CCNE1. Frequency of CCNE1 amplification in the top 7 TCGA tumor types is summarized in the bar graph. Abbreviations are based on the TCGA naming convention: BLCA, bladder urothelial cancer; OV, ovarian serous cystadenocarcinoma; SARC, sarcoma; STAD, stomach adenocarcinoma; UCEC, uterine corpus epithelium carcinoma; UCS, uterine carcinosarcoma.

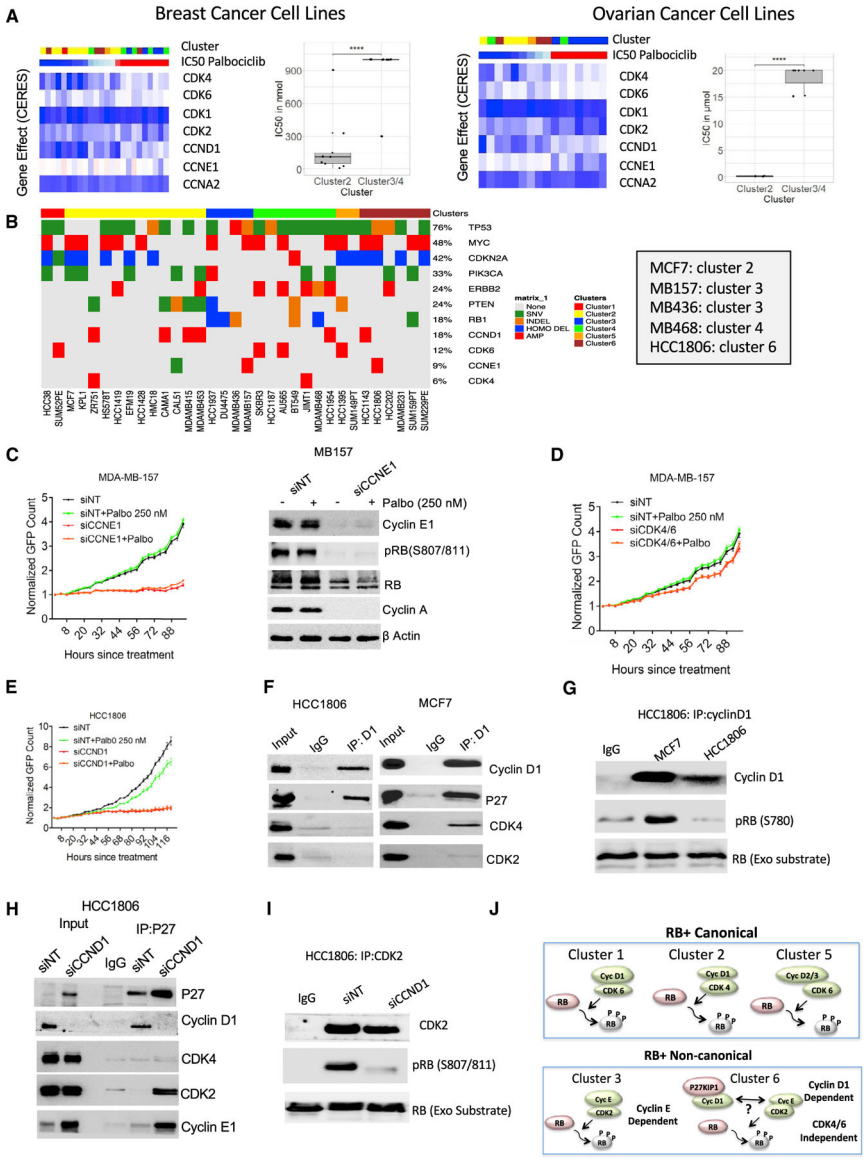

Figure 3. Differential CDK/cyclin requirements in RB-proficient models

(A) Color bar shows clusters organized by IC_{50} of palbociclib with the relative sensitivity to the indicated CDK and cyclin genes depicted in the heatmap for breast and ovarian cancer cell lines. Boxplots summarize the IC_{50} from the indicated clusters (****$p < 0.0001$ as determined by t test).

(B) Oncoprint depicts genetic features of breast cancer cell lines relative to the clustering. Specific cell lines used functionally are summarized in the box.

(C) Live cell imaging was used to explore the impact of CCNE1 knockdown in the absence and presence of palbociclib in the MB157 cell line. Error bars indicate means and SDs from triplicate, and experiments were done at 2 independent times. Biochemical characterization of the effect of CCNE1 knockdown in the MB157 cell model.

(D–F) Live cell imaging to monitor the growth of MB157 in the absence and presence of palbociclib following CDK4/6 knockdown (D). The means and SDs are shown. The

experiment was performed in triplicate. (E) Live cell imaging on HCC1806 cells to determine the effect of CCND1 knockdown in the presence or absence of palbociclib. Means and SDs were calculated and the experiments were done in triplicate at 2 independent times. (F) Complex formation between cyclin D1 and other CDKs and $p27^{KIP1}$ in HCC1806 and MCF7 cell lines was determined by co-immunoprecipitation.
(G) Immunoprecipitated cyclin D1 from MCF7 and HCC1806 cells was used in kinase reactions against an exogenous RB substrate. Kinase activity is measured by RB phosphorylation.
(H) Immunoprecipitation in HCC1806 cells following CCND1 knockdown was performed. Co-immunoprecipitated proteins were determined by western blotting.
(I) Immunoprecipitated CDK2 from HCC1806 cells with cyclin D1 depleted by RNAi or with a non-targeting RNAi poll (SiNT) was used for kinase reactions against an exogenous RB substrate. Kinase activity is measured by RB phosphorylation.
(J) Schematic of different RB-proficient cell cycles operable in breast cancer models.

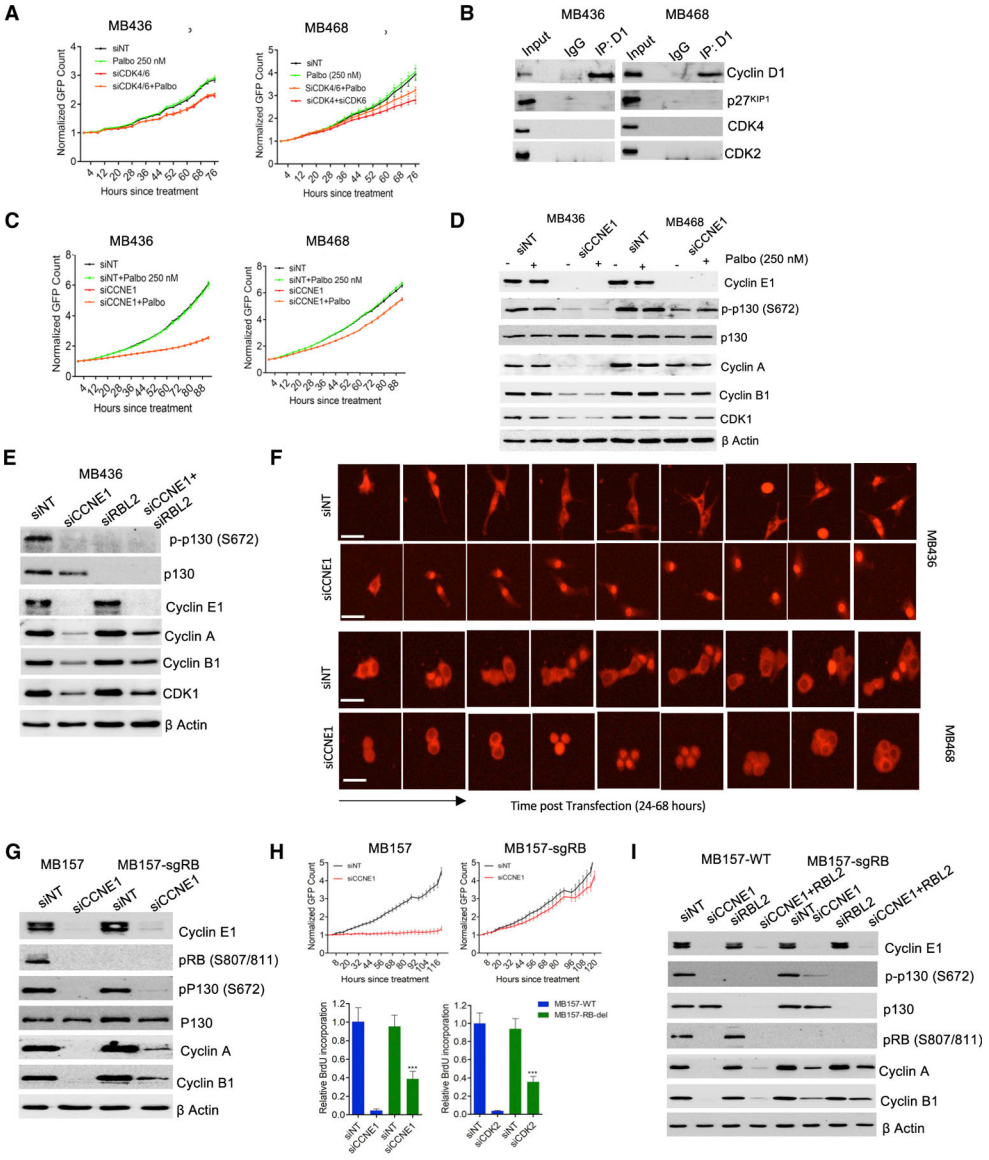

Figure 4. Differential requirements of RB-deficient cells on cyclin E and p130

(A and B) Live cell imaging to track the division of MB436 and MB468 cells treated with palbociclib and/or the knockdown of CDK4 and CDK6 (A). Means and SDs are shown and calculated from triplicate. (B) Co-immunoprecipitation of cyclin D1 showing the failure to assemble complexes with the indicated proteins.

(C) Live cell imaging to demonstrate the differential effect of CCNE1 knockdown in MB436 and MB468 cell lines in the presence or absence of palbociclib. Error bars indicate means and SDs. Experiments were done in triplicate and repeated at 2 independent times.

(D) Biochemical characterization of the differential effect of CCNE1 knockdown in MB436 and MB468 cell models.

(E) Biochemical analysis of the impact of CCNE1 and RBL2 knockdown on cell-cycle proteins.

(F) Live-cell imaging to track the localization of CDK2 sensor in the nucleus and cytoplasm at the indicated time points in MB436 and MB468 cell lines following CCNE1 knockdown (nuclear localization indicates low kinase activity and cytoplasmic localization indicates high kinase activity; scale bar, 50 μm).

(G) MB157 parental model and model with RB deleted were used to evaluate the effect of CCNE1 knockdown on the indicated proteins by immunoblotting.

(H) Live-cell imaging and BrdU incorporation assay were performed in MB157 cell line to delineate the effect of RB deletion on the sensitivity to CDK2 or CCNE1 knockdown. Column represents means and SDs from 3 independent experiments (***$p < 0.001$ as determined by Student's t test).

(I) The indicated proteins were detected in the MB157 parental model or the RB-deleted variant with CCNE1 and RBL2 knockdown.

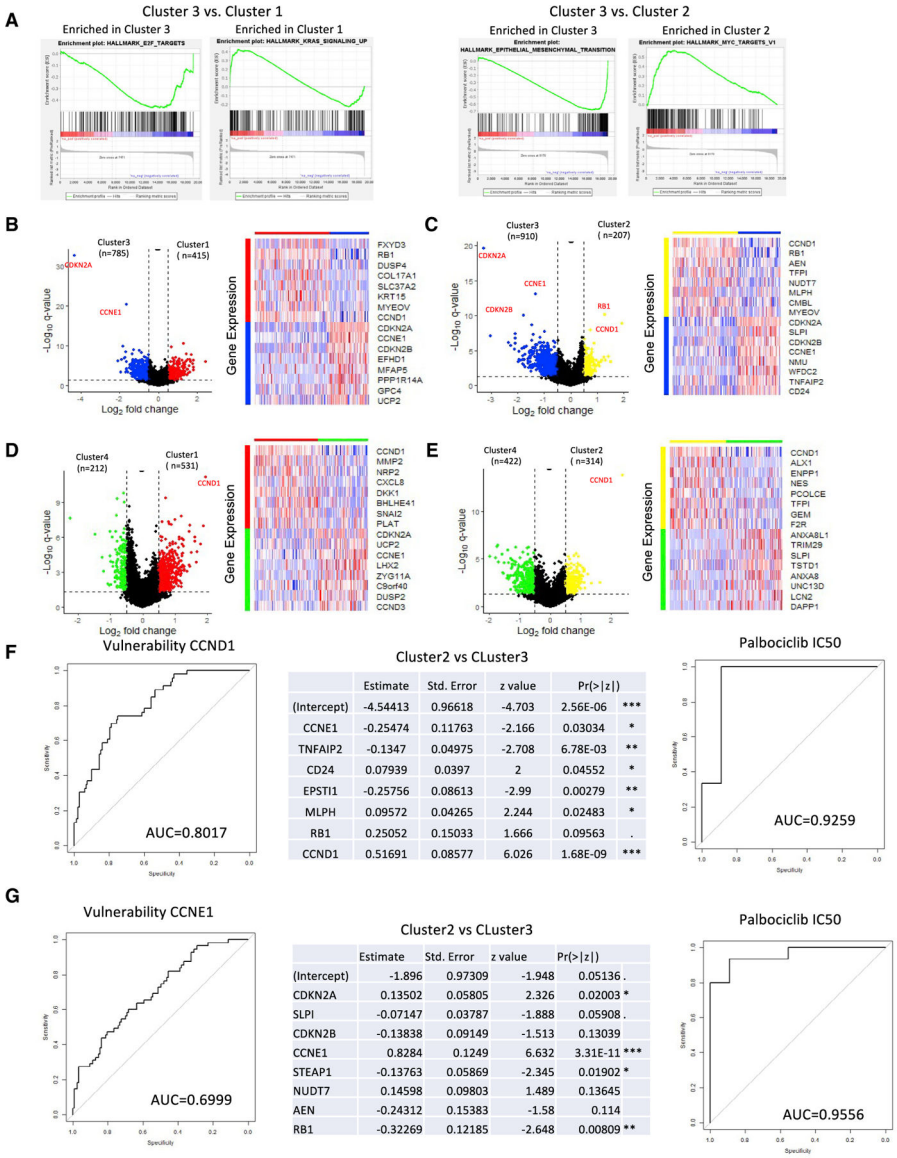

	Estimate	Std. Error	z value	Pr(>|z|)	
(Intercept)	-4.54413	0.96618	-4.703	2.56E-06	***
CCNE1	-0.25474	0.11763	-2.166	0.03034	*
TNFAIP2	-0.1347	0.04975	-2.708	6.78E-03	**
CD24	0.07939	0.0397	2	0.04552	*
EPSTI1	-0.25756	0.08613	-2.99	0.00279	**
MLPH	0.09572	0.04265	2.244	0.02483	*
RB1	0.25052	0.15033	1.666	0.09563	.
CCND1	0.51691	0.08577	6.026	1.68E-09	***

	Estimate	Std. Error	z value	Pr(>|z|)	
(Intercept)	-1.896	0.97309	-1.948	0.05136	.
CDKN2A	0.13502	0.05805	2.326	0.02003	*
SLPI	-0.07147	0.03787	-1.888	0.05908	.
CDKN2B	-0.13838	0.09149	-1.513	0.13039	
CCNE1	0.8284	0.1249	6.632	3.31E-11	***
STEAP1	-0.13763	0.05869	-2.345	0.01902	*
NUDT7	0.14598	0.09803	1.489	0.13645	
AEN	-0.24312	0.15383	-1.58	0.114	
RB1	-0.32269	0.12185	-2.648	0.00809	**

Figure 5. Gene expression features are associated with different CDK-cyclin vulnerabilities

(A) GSEA analysis was used to define enriched ‘‘hallmark’’ gene sets based on ranked gene expression differences between the clusters. Representative top enrichments plots are shown.

(B–E) Differential gene expression analyses were performed using the gene expression data from all of the cell lines for the indicated clusters. The number of cell lines in each cluster used: cluster 1, n = 133; cluster 2, n = 105; cluster 3, n = 68; and cluster 4, n = 103. Volcano plots summarize the gene distribution, and top genes of significance are indicated in red font (log fold-change cutoff >0.5 and $p < 0.05$). Top eight up-/downregulated genes are summarized in the heatmaps.

(F and G) Logistic regression used the top genes that were different between clusters 2 and 3 to define a classifier for vulnerability to CCND1 or CCNE1 depletion. Receiver operating characteristic (ROC) curves and classifier are shown. The subsequent ability of that classifier to predict sensitivity to palbociclib in breast cancer samples is shown in the ROC curves.

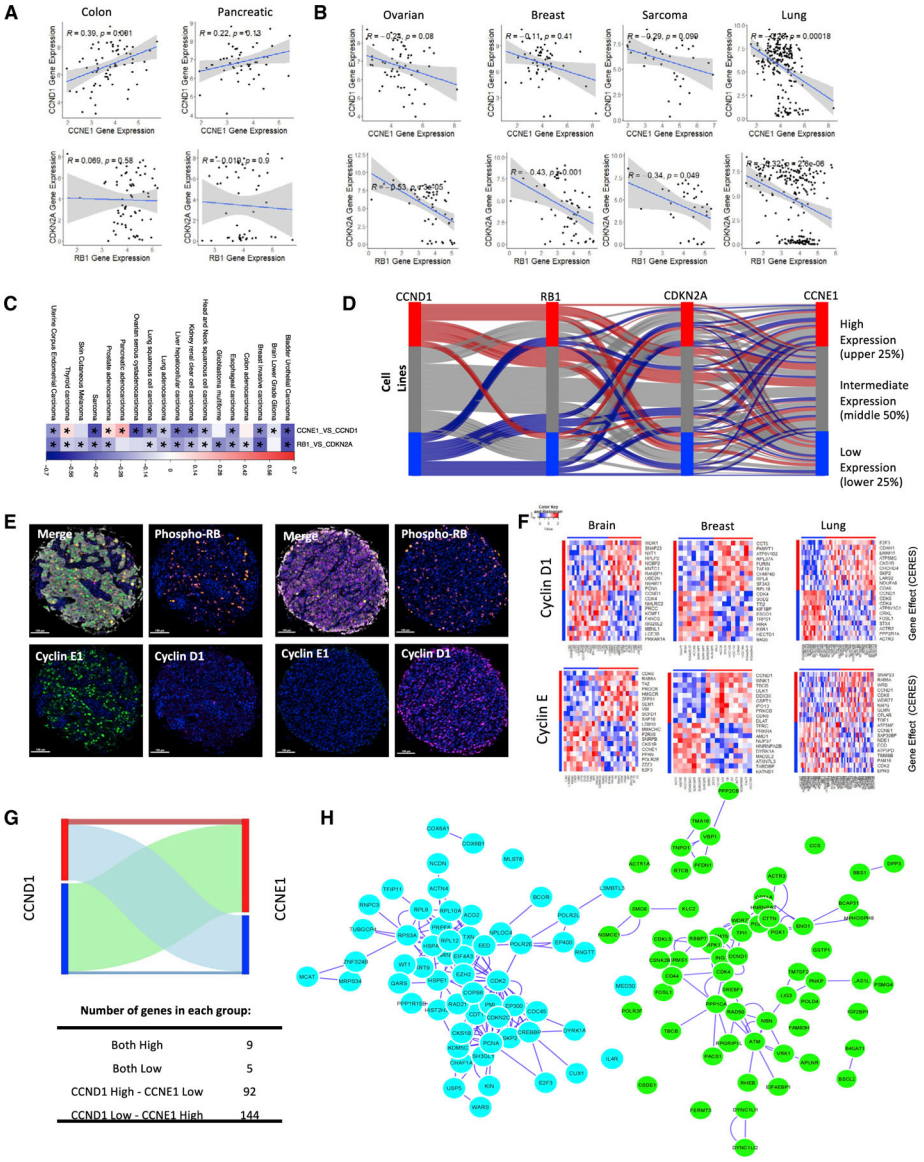

Figure 6. Cell-cycle features define different tumor classes

(A) In colon and pancreatic cancer cell lines, there is a positive relationship between CCND1 and CCNE1 and no correlation between RB and CDKN2A. The correlation coefficient and related p valuate are shown.

(B) In other tumor types (e.g., ovarian, breast, sarcoma, lung), there is a reciprocal relationship of CCND1/CCNE1 and RB1/CDKN2A, suggesting distinct cell-cycle states in different tumors. The correlation coefficient and related p values are shown.

(C) Analysis of TCGA data (pan-cancer release) relative to the relationship of CCNE1/CCND1 and RB/CDKN2A in cancers. In most of the tumor types indicated, there is a reciprocal relationship (color bar shows correlation coefficient and * denotes significance).

(D) Sankey analysis of solid tumor clusters (n = 574) shows the relationship between cell lines in different expression quantiles.

(E) Multispectral staining showing different RB-proficient cell cycles dominated by cyclin E or cyclin D1. Representative images are shown (scale bar, 100 μm).
(F) Heatmaps show the top vulnerabilities in the indicated tumor type based on the expression of CCND1 or CCNE1.
(G) Sankey plots demonstrate the sensitivity/resistance behavior to gene depletion based on the expression of CCND1 compared with CCNE1.
(H) Network analyses of gene differentially required in CCND1 high (green) compared with CCNE1 high (teal) tumor cell lines.

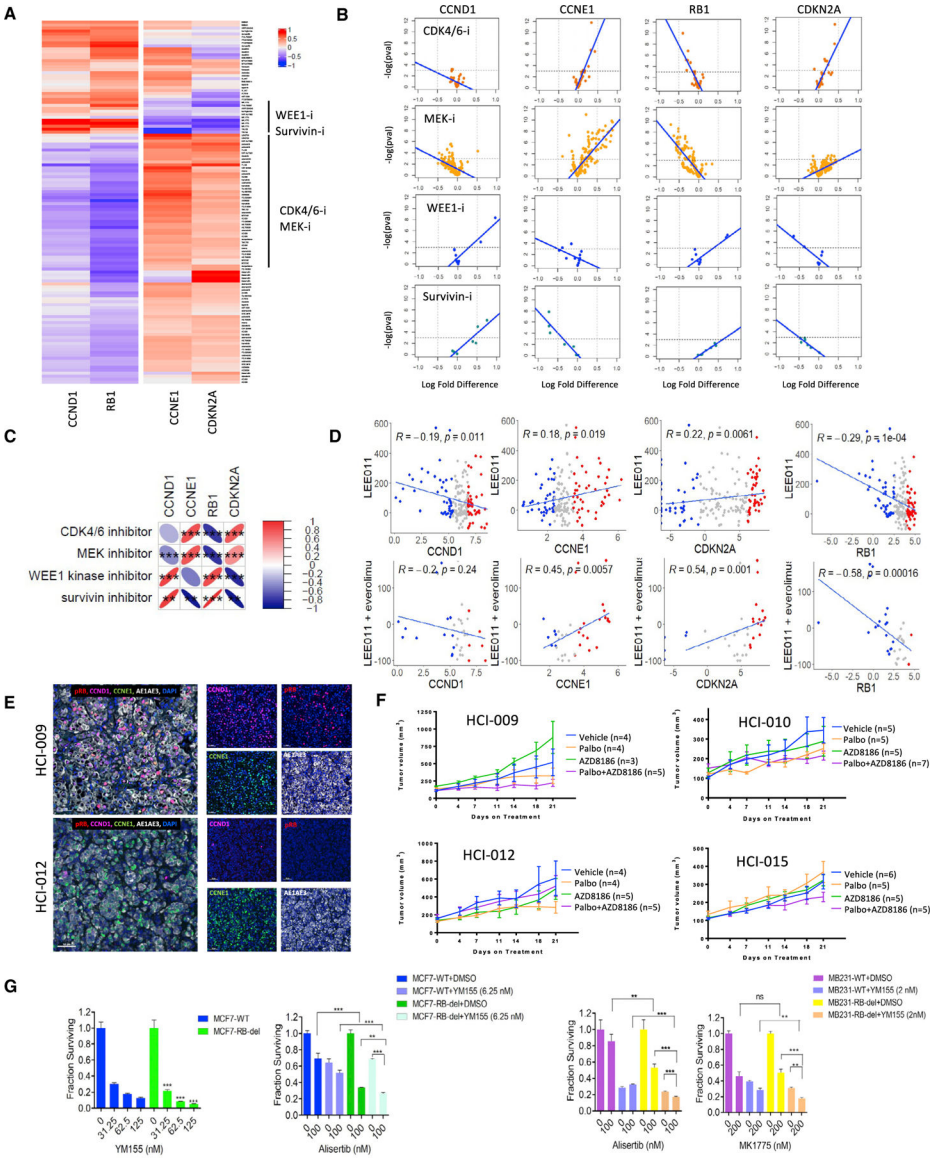

Figure 7. Drug responses show reciprocal relationships based on cell-cycle states

(A) Heatmap showing drugs with reciprocal response relationships between groups of cell lines with high and low expression in CCND1/RB1 and CCNE1/CDKN2A (determined using upper and lower expression quantiles; N = 71 in each quantile group, N = 140 in the intermediate group). Values shown are the ratio between mean drug response of cell lines with high gene expression compared to mean drug response of cell lines with low gene expression (color bar is the log fold-change [logFC] in the comparison groups).

(B) Volcano plots with trend lines showing the correlation between drug response log fold-changes and p values across each gene for specific drug families.

(C) Correlation plot showing drug family response trendline correlation coefficients and p values (*p < 0.05, **p < 0.01, ***p < 0.001).

(D) Correlation between CCND1, CCNE1, RB1, and CDKN2A gene expression, with drug sensitivity in PDX models. PDX models with gene expression greater than the 75th

percentile are marked in red and models with gene expression less than the 25th percentile are marked in blue. PDX models that have no information regarding drug sensitivity were removed. The correlation coefficient and related p valuate are shown.

(E) Representative multispectral staining for PDX models that are RB proficient (HCI-009) and RB deficient (HCI-012) (scale bar, 100 mm).

(F) The indicated PDX models were treated with CDK4/6 (palbociclib) and/or mTOR (AZD8186) inhibitor, and the effect on tumor growth was measured by calipers. The number of mice for each treatment group is shown, and the means and SEMs are plotted.

(G) The effect of the indicated drugs and combinations were evaluated in isogenic MCF7 and MB231 cells harboring RB deletion. Cell viability was determined using the CellTiter-Glo (CTG) assay. The column represents means and SDs from triplicates (**$p < 0.01$, ***$p < 0.001$ as determined by Student's t test).

KEY RESOURCES TABLE

REAGENT or RESOURCE	SOURCE	IDENTIFIER
Antibodies		
Rabbit monoclonal anti-pRB (Ser807/811)(D20B12)	Cell Signaling Technology	Cat# 8516, RRID:AB_11178658
Rabbit monoclonal anti-pRB (Ser780)	Cell Signaling Technology	Cat# 9307, RRID:AB_330015
Mouse monoclonal anti-RB (4H1)	Cell Signaling Technology	Cat# 9309, RRID:AB_823629
Rabbit monoclonal anti-CDK2 (78B2)	Cell Signaling Technology	Cat# 2546, RRID:AB_2276129
Rabbit monoclonal anti-CDK4 (D9G3E)	Cell Signaling Technology	Cat# 12790, RRID:AB_2631166
Mouse monoclonal anti-CDK6 (DCS83)	Cell Signaling Technology	Cat# 3136, RRID:AB_2229289
Mouse monoclonal anti-Cyclin E1(HE12)	Cell Signaling Technology	Cat# 4129, RRID:AB_2071200
Rabbit monoclonal anti-P27KIP1 (D69C12)	Cell Signaling Technology	Cat# 3686, RRID:AB_2077850
Rabbit monoclonal anti-Cyclin B1(D5C10)	Cell Signaling Technology	Cat# 12231, RRID:AB_2783553
Rabbit monoclonal anti-p130 (D9T7M)	Cell Signaling Technology	Cat# 13610, RRID:AB_2798274
Mouse IgG1 Isotype control (G3A1)	Cell Signaling Technology	Cat# 5415, RRID:AB_10829607
Normal rabbit IgG	Cell Signaling Technology	Cat# 2729, RRID:AB_1031062
Mouse monoclonal anti-Cyclin D1(DCS-6)	Santacruz Biotechnology	Cat# sc-20044, RRID:AB_627346
Mouse monoclonal anti-cyclin D1 (DCS-11)	Thermo Scientific	Cat# MA5–12707, RRID:AB_10986118
Goat anti-rabbit IgG Secondary antibody HRP	Thermo Scientific	Cat# A27036, RRID:AB_2536099
Mouse monoclonal anti-Cyclin A (B-8)	Santacruz Biotechnology	Cat# sc-271682, RRID:AB_10709300
Mouse monoclonal anti-CDK1 (17)	Santacruz Biotechnology	Cat# sc-54, RRID:AB_627224
Mouse monoclonal anti-β Actin (C4)	Santacruz Biotechnology	Cat# sc-47778 HRP, RRID:AB_2714189
Mouse monoclonal anti-GAPDH (0411)	Santacruz Biotechnology	Cat# sc-47724, RRID:AB_627678
m-IgGk BP-HRP	Santacruz Biotechnology	Cat# sc-516102, RRID:AB_2687626
Rabbit monoclonal anti-Cyclin D1 (SP4)	Epredia	Cat# RM-9104-S1, RRID:AB_149913
Rabbit monoclonal anti-Cyclin E1 (EP435E)	Abcam	Cat# ab33911, RRID:AB_731787
Rabbit monoclonal anti-phospho p130 (S672)	Abcam	Cat# ab76255, RRID:AB_2284799
Rabbit monoclonal anti-MCM2 (RBT-MCM2)	Bio SB	Cat# BSB 6334, RRID N/A
Mouse monoclonal anti-human cytokeratin (AE1AE3)	Agilent DAKO	Cat# M3515, RRID:AB_2132885

REAGENT or RESOURCE	SOURCE	IDENTIFIER
Rabbit polyclonal anti-pHH3 (Ser10)	Millipore Sigma	Cat# 06–570, RRID:AB_310177
Biological samples		
Triple negative breast cancer TMA	Witkiewicz lab; Roswell park cancer Center	NA
Welm PDX model	Welm Lab, Huntsman Cancer Institute, University of Utah	NA
Chemicals, peptides, and recombinant proteins		
AZD8186	Selleckchem	S7694
Palbociclib	MedChem express	HY-50767A
YM155	Selleckchem	S1130
Alisertib	Selleckchem	S1133
Pemetrexed	Selleckchem	S1135
Navitoclax	Selleckchem	S1001
Dimethyl Sulfoxide	Fisher Scientific	BP231–100
Protein A agarose beads	Thermo Scientific	20333
Protein G agarose beads	Thermo Scientific	20399
Lipofectamine RNAimax	Thermo Scientific	13778–150
Critical commercial assays		
Chemiluminescent ELISA BrdU incorporation assay	Sigma	11669915001
Cell titer-Glo (CTG) Luminescent cell viability assay	Promega	G7573
ProtoGlow ECL	National Diagnostics	CL-300
Deposited data		
DepMap gene dependency data, RNA seq, mutation, copy number, and cell line sample information	DepMap	https://depmap.org/portal/download/
TCGA datasets were acquired from cBioportal from the PanCancer Atlas Study	cBioportal	https://www.cbioportal.org/datasets
Experimental models: Cell lines		
HCC1806	ATCC	Cat# CRL-2335, RRID:CVCL_1258
MB436	ATCC	Cat# HTB-130, RRID:CVCL_0623
MB468	ATCC	Cat# HTB-132, RRID:CVCL_0419
MCF7	ATCC	Cat# HTB-22, RRID:CVCL_0031
MB231	ATCC	Cat# CRM-HTB-26, RRID:CVCL_0062
MB-157	ATCC	Cat# CRL-7721, RRID:CVCL_0618
Experimental models: Organisms/strains		
NSG mice	Jackson Labs	5557
Oligonucleotides		
On-TARGETplus Human CCNE1 siRNA SMARTpool	Horizon Discovery	L-003213–00-0005

REAGENT or RESOURCE	SOURCE	IDENTIFIER
On-TARGETplus Human CCND1 siRNA SMARTpool	Horizon Discovery	L-003210–00-0005
On-TARGETplus Human CDK4 siRNA SMARTpool	Horizon Discovery	L-003238–00-0005
On-TARGETplus Human CDK6 siRNA SMARTpool	Horizon Discovery	L-003240–00-0005
On-TARGETplus Human CDKN1B siRNA SMARTpool	Horizon Discovery	L-003472–00-0005
On-TARGETplus Human CDK2 siRNA SMARTpool	Horizon Discovery	L-003236–00-0005
On-TARGETplus Human CCNA2 siRNA SMARTpool	Horizon Discovery	L-003205–00-0005
On-TARGETplus Human RBL2 siRNA SMARTpool	Horizon Discovery	L-003299–00-0005
On-TARGETplus Nontargeting control Pool	Horizon Discovery	D-001810–10-05
Recombinant DNA		
CSII-EF lentiviral vector, cDNA for HDHB-mCHERRY	Spencer Lab	N/A
pLenti0.3UbCGWH2BC1-PatGFP	Abel lab; Roswell Park cancer Center	N/A
pL-CRIPSR-EFS-sgCtrl-tRFP	Bremner Lab; Lunenfeld-Tanenbaum Research Institute	N/A
Software and algorithms		
Prism	Graphpad.com	V7
FCS express	deovosoftware.com	V7
inForm® Software	AKOYA Biosciences	v2.4.11
R Studio	RStudio.com	N/A
Gene Set Enrichment Analysis (GSEA)	ftp.broadinstitute.org://pub/gsea/gene_sets/h.all.v7.4.symbols.gmt ftp.broadinstitute.org://pub/gsea/annotations_versioned/ Human_Gene_Symbol_with_Remapping_MSigDB.v7.4.chip	v4.1.0
Protein-protein interaction network	Biogrid	Homo sapiens, v. 3.5.168